

Chiral anomaly and high-energy scattering in QCD

Alan R. White*

High Energy Physics Division, Argonne National Laboratory, 9700 South Cass Avenue, Argonne, Illinois 60439

(Received 4 April 2002; published 23 September 2002)

Infrared properties of the triangle anomaly and the “anomaly pole” are elaborated and applied to the study of high-energy scattering in QCD, when the gauge symmetry is partially broken to SU(2). It is shown that the chiral flavor anomaly provides a wee-gluon component for Goldstone bosons that combines with interactions due to the U(1) anomaly to produce an infrared transverse momentum scaling divergence in scattering amplitudes. After the divergence is factorized out, as a wee-gluon condensate in the infinite momentum pion, the remaining physical amplitudes have confinement and chiral symmetry breaking. A lowest-order contribution to the pion scattering amplitude is calculated in detail. Although originating from very complicated diagrams, the amplitude has a remarkable (semi)perturbative simplicity. The momentum structure is that of single gluon exchange but zero transverse momentum quarks inject additional spin and color structure via anomaly interactions.

DOI: 10.1103/PhysRevD.66.056007

PACS number(s): 11.15.Bt, 11.55.Fv, 11.55.Jy

I. INTRODUCTION

Any solution of the full Regge limit of QCD must, almost certainly, involve a resolution of the unsolved problem of matching perturbation theory with confinement. Since the limit involves large energies its description should not be too far from perturbation theory. Conversely, since small momentum transfers are involved, both confinement and chiral symmetry breaking must be manifest in the contribution of physical t -channel states. In this paper we will show that a transition from perturbation theory to confinement can indeed occur in the Regge region.

For some time we have pursued what might be called a “semiperturbative” description of the QCD Pomeron. In doing so we have made extensive use of the formalism of (multi-)Regge theory, which many authors currently studying the Pomeron make little or no reference to. In this paper we endeavor to keep, at least the most unfamiliar parts of, this formalism to a minimum. Nevertheless, we can summarize the reasons why we believe that Regge poles and Regge theory must play a fundamental role in solving the Regge limit of QCD as follows.

In general, multiparticle t -channel unitarity has been shown to be satisfied when the only J -plane singularities are Regge poles and the Regge cuts generated by them—provided the Regge cut discontinuities satisfy “Reggeon unitarity” [1–3]. No other solution is known. It is well established [4–9] that when the gauge symmetry of QCD is spontaneously broken, multi-Regge limits of quark and gluon amplitudes are described perturbatively by Reggeon diagrams containing massive gluon and quark Regge poles. Both t -channel (Reggeon) unitarity and s -channel unitarity are satisfied. General arguments imply that the small transverse momentum part of the massless theory can be obtained smoothly from the massive theory. In which case, the unitarity properties of the massive theory, including Reggeon unitarity, should persist in the massless theory. [Note that the

Balitskiĭ-Fadin-Kuraev-Lipatov (BFKL) Pomeron, which is not a Regge pole and also does not satisfy s -channel unitarity, is a large transverse momentum phenomenon that appears only when a subclass of diagrams is isolated and summed to all orders—without a transverse momentum cut-off.]

The critical Pomeron [10] is an abstract solution of Reggeon unitarity, obtained via Reggeon field theory (RFT), that produces asymptotically rising cross sections. A single Regge pole and the corresponding Regge cuts are the only J -plane singularities. Since the critical Pomeron retains the factorization properties of a single Regge pole, if it occurs in QCD it will be associated [11] with a “universal wee-parton distribution” in hadrons. This universality property allows wee partons to carry vacuum properties which, in combination with rising cross sections, should lead to the maximal asymptotic applicability of the parton model.

We expect the occurrence of the critical Pomeron in QCD to be of crucial importance, therefore, both for the satisfaction of t -channel unitarity and for the maximal validity of the parton model. To see that it can indeed occur we have proposed [9,11,12] starting with the gluon and quark Reggeon diagrams of spontaneously broken QCD. With a transverse momentum cutoff imposed, the gauge symmetry can be restored in stages and RFT can be used to analyze the infrared divergences that occur. We have anticipated that the only additional ingredient beyond the perturbative Regge behavior of gluons and quarks will be chirality transitions produced by the fermion anomaly. Quarks will, therefore, play an essential role.

We have now shown that chirality transitions occur [13–15] in effective triangle diagram Reggeon interactions obtained by placing quark lines on-shell in large quark loops. These interactions appear in the Reggeon vertices that couple different Reggeon channels (in a general multi-Regge limit). In particular, they occur in the triple-Regge vertex [16] that couples three distinct Reggeon channels—each carrying a separate transverse momentum. Such vertices include the couplings of bound-state Reggeons (e.g. pions and nucleons) together with their couplings to the physical Pomeron. Effec-

*Email address: arw@hep.anl.gov

tively, therefore, vertices of this kind determine the bound states of the theory and their high-energy scattering amplitudes.

Our expectation has long been that when the gauge symmetry is restored first to $SU(2)$, giving “color superconducting QCD,” $SU(2)$ color confinement will be due to the appearance of a condensate in Reggeon states produced by infrared divergent “wee-gluon” configurations coupling through anomaly interactions. The resulting Pomeron could then be in a supercritical phase [2] of RFT, implying that the critical Pomeron would occur as the full $SU(3)$ gauge symmetry is restored (provided the transverse cutoff can be removed first—a strong requirement). *A priori*, however, to understand in detail how the anomaly interactions produce the condensate, and determine both hadron states and the Pomeron, it is necessary to self-consistently construct the full multi-Regge S matrix. This is a very complicated project to carry out. We outlined, essentially, how it could be done in [15], although we did not then have the full knowledge of anomaly vertices that we now have.

In this paper, as an intermediate step before attempting to construct the full multi-Regge S matrix, we approach the problem from a different standpoint. We use a procedure that is less rigorously formulated (as will become apparent) than the multi-Regge approach. However, it leads directly to explicit results and provides a straightforward understanding of the physics that is involved. Also the terminology used is, we hope, more widely familiar. The new approach is not only sufficient to show how, in infinite momentum scattering, anomalies determine both the physical states and the exchanged Pomeron, but it also allows us to obtain explicit high-energy scattering amplitudes. In fact, we directly calculate the on-shell (massless) pion amplitude rather than the amplitude for spacelike Reggeized pions to scatter, that multi-Regge theory would lead us to try to calculate.

We start directly from infrared properties of the triangle diagram. It is well known [17–21] that, when the quarks involved are massless, the chiral flavor anomaly requires that an “anomaly pole” appear in the vertices for an axial current to couple to pairs of vector currents carrying lightlike momenta. If there is confinement and the chiral symmetry is broken spontaneously this pole becomes a physical Goldstone pole. In Sec. II we study in detail how the pole is generated in the triangle diagram and show that, in the momentum configuration involved, one propagator carries zero momentum (and undergoes a chirality transition) while the other two carry the external light-cone momenta. We also show that while the tensor coupling of the anomaly pole necessarily vanishes on-shell at finite momentum, an on-shell coupling potentially exists at infinite momentum.

In Sec. III we show that in color superconducting QCD the role of light-cone momenta in producing the anomaly pole implies the existence of crucial wee-gluon effective

couplings for Goldstone bosons at infinite momentum. (The massive gluons produced by the color symmetry breaking are essential for the existence of these couplings.) As a result, the quark-antiquark “pion” and quark-quark (or antiquark-antiquark) “nucleon” Goldstone states that appear [22] have just the (massless) wee gluon content that we envisaged emerging from our general Reggeon diagram analysis. The presence of the wee gluons then leads directly to the contribution of $U(1)$ anomaly Reggeon interactions in the high-energy scattering of pions (and nucleons). An overall logarithmic divergence is produced that selects anomaly mediated scattering as the dominant physical process. The divergence can be factorized off as the expected “condensate” within the scattering pions—with the residue being the physical scattering amplitude. The “anomaly pole” is manifest as a transverse momentum δ -function that factorizes the momentum dependence of the divergent wee gluon interactions and the “parton interaction” of the massive sector of the theory.

The lowest-order contribution to the pion scattering amplitude has a remarkable simplicity. The momentum structure is just that of lowest-order gluon exchange. However, zero momentum quarks inject spin and color structure (via anomaly interactions) that modifies the signature and color symmetry properties of the amplitude. Because of the complexity of the initial diagrams and the resulting reduction process we limit the presentation, in this paper, to an “existence proof” that demonstrates how the kinematical and dynamical properties of the chiral flavor and $U(1)$ anomalies actually combine with transverse momentum divergences to produce physical amplitudes. To do this we follow the reduction process through in detail for just one of the diagrams involved.

In Sec. IV we discuss both the conclusions that can be drawn from our results and the further work that needs to be done to establish the relationship of the critical Pomeron to QCD. We also discuss some more general issues of principle.

II. PROPERTIES OF THE TRIANGLE GRAPH

In our previous paper [14] we based our infrared anomaly analysis on the rather abstract discussions of [18] and [19]. In this paper we will use explicit evaluations of the triangle graph (in particular kinematic configurations) that exist in the literature [20,21]. In the following we summarize and expand the results and properties we will use. We will particularly emphasize the important role of (both external and internal) light-cone momenta in the infrared properties that we exploit.

A. Invariant amplitudes and Ward identities

We consider the elementary triangle diagram amplitude

$$\Gamma_{\mu\alpha\beta}(k_1, k_2) = \frac{1}{(2\pi)^4} \int d^4p \frac{\text{Tr}\{\gamma_5 \gamma_\mu(\mathbf{k}_2 - \mathbf{p}) \gamma_\alpha(-\mathbf{k}_1 + \mathbf{k}_2 - \mathbf{p}) \gamma_\beta(-\mathbf{k}_1 - \mathbf{p})\}}{(p + k_1 - k_2)^2 (k_2 - p)^2 (p + k_1)^2} \quad (2.1)$$

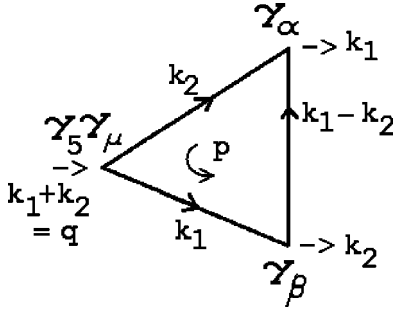


FIG. 1. Triangle diagram notation.

where the notation is illustrated in Fig. 1. The significance of routing the external momenta as we have done will be discussed shortly. The amplitude

$$T_{\mu\alpha\beta}(k_1, k_2) = \Gamma_{\mu\alpha\beta}(k_1, k_2) + \Gamma_{\mu\beta\alpha}(k_2, k_1) \quad (2.2)$$

is the lowest order interaction of the axial vector current $A_\mu(q)$, where $A_\mu = \bar{\psi} \gamma_5 \gamma_\mu \psi$ and the vector currents, $V_\alpha(k_1)$ and $V_\beta(k_2)$, where $V_\mu = \bar{\psi} \gamma_\mu \psi$ and ψ is a massless fermion field. $T_{\mu\alpha\beta}$ can be decomposed into invariant amplitudes by writing

$$\begin{aligned} T_{\mu\alpha\beta}(k_1, k_2) = & A_1 \epsilon_{\sigma\alpha\beta\mu} k_1^\sigma + A_2 \epsilon_{\sigma\alpha\beta\mu} k_2^\sigma + A_3 \epsilon_{\delta\sigma\alpha\mu} k_{1\beta} k_1^\delta k_2^\sigma \\ & + A_4 \epsilon_{\delta\sigma\alpha\mu} k_{2\beta} k_1^\delta k_2^\sigma + A_5 \epsilon_{\delta\sigma\beta\mu} k_{1\alpha} k_1^\delta k_2^\sigma \\ & + A_6 \epsilon_{\delta\sigma\beta\mu} k_{2\alpha} k_1^\delta k_2^\sigma. \end{aligned} \quad (2.3)$$

Bose symmetry implies

$$T_{\mu\alpha\beta}(k_1, k_2) = T_{\mu\beta\alpha}(k_2, k_1) \quad (2.4)$$

and so requires that

$$\begin{aligned} A_1(k_1, k_2) &= -A_2(k_2, k_1) \\ A_3(k_1, k_2) &= -A_6(k_2, k_1) \\ A_4(k_1, k_2) &= -A_5(k_2, k_1). \end{aligned} \quad (2.5)$$

In addition, the vector Ward identities

$$k_1^\alpha \Gamma_{\mu\alpha\beta} = 0, \quad k_2^\beta \Gamma_{\mu\alpha\beta} = 0 \quad (2.6)$$

require

$$A_2 = k_1^2 A_5 + k_1 \cdot k_2 A_6 \quad (2.7)$$

$$A_1 = k_2^2 A_4 + k_1 \cdot k_2 A_3. \quad (2.8)$$

A priori, a term of the form

$$A(k_1, k_2) \epsilon_{\delta\sigma\alpha\beta} k_1^\delta k_2^\sigma (k_1 + k_2)_\mu \quad (2.9)$$

with $A(k_2, k_1) = -A(k_1, k_2)$, could be added to Eq. (2.3). Such a term separately satisfies the Ward identities (2.6). However, because of the identity

$$\begin{aligned} \epsilon_{\delta\sigma\alpha\beta} k_1^\delta k_2^\sigma [k_1 + k_2]_\mu = & -(\epsilon_{\delta\sigma\alpha\mu} k_{1\beta} - \epsilon_{\delta\sigma\beta\mu} k_{2\alpha} - \epsilon_{\delta\sigma\beta\mu} k_{1\alpha} \\ & + \epsilon_{\delta\sigma\beta\mu} k_{2\beta}) k_1^\delta k_2^\sigma + \epsilon_{\sigma\alpha\beta\mu} k_2^\sigma (k_1 \cdot k_2 \\ & - k_1^2) - \epsilon_{\sigma\alpha\beta\mu} k_1^\sigma (k_1 \cdot k_2 - k_2^2) \end{aligned} \quad (2.10)$$

Eq. (2.9) can be re-expressed in the form (2.3). As we will see, the identity (2.10) can be used [20] to simplify Eq. (2.3) in many special kinematic situations. Note that, with A a constant, Eq. (2.9) does not satisfy Bose symmetry. Nevertheless, in asymmetric momentum configurations it can, effectively, appear with a constant coefficient. This will be important for the discussion later in this section.

We define the integral (2.1) as the limit $m \rightarrow 0$ of that in which a fermion mass m is added. Equations (2.3) and (2.5) hold also when $m \neq 0$ and ultraviolet regularization can be carried out with Eqs. (2.7) and (2.8) maintained. Indeed, it is well known that the Ward identities (2.6) can be regarded as a consequence of routing the external momenta as we have done in Fig. 1. An ‘‘anomaly’’ then appears in the Ward identity for the axial current. Since only the A_1 and A_2 terms in Eq. (2.3) contribute to the axial current divergence, the anomaly has to appear in these terms. In fact, ultraviolet regularization of Eq. (2.1) directly produces the contribution

$$T_{\mu\alpha\beta}(k_1, k_2) = \frac{1}{4\pi^2} \epsilon_{\sigma\alpha\beta\mu} k_1^\sigma + \frac{1}{4\pi^2} \epsilon_{\sigma\alpha\beta\mu} k_2^\sigma + \dots \quad (2.11)$$

leading to the divergence equation (when $m=0$)

$$(k_1 + k_2)^\mu T_{\mu\alpha\beta} = \frac{1}{2\pi^2} \epsilon_{\delta\sigma\alpha\beta} k_1^\delta k_2^\sigma. \quad (2.12)$$

The (coefficient on the) right-hand side of Eq. (2.12) is commonly referred to as ‘‘the anomaly.’’ Even though the anomaly occurs only in A_1 and A_2 the vector Ward identities (2.7) and (2.8) require related terms to appear in the other A_i . We will be particularly concerned with the infrared behavior of the massless A_i that is required [18,19].

B. Explicit formulas for the A_i

No (nonintegral) analytic expression for the full amplitude (2.1) exists in the literature. However, it is possible to give explicit expressions in limited kinematic configurations. For example, when $k_1^2 = k_2^2$ the imaginary parts of each of the invariant amplitudes A_i is given in [20]. For our purposes we will use the following set of formulas, given in [21], for the full amplitudes.

When $k_1^2=0$ ($k_2^2, q^2 < 0, m^2 > 0$),

$$\begin{aligned}
A_6 &= -A_3 = -\frac{1}{2\pi^2} \frac{1}{k_2^2 - q^2} \left(\frac{k_2^2}{k_2^2 - q^2} L_1 - \frac{m^2}{k_2^2 - q^2} L_2 - 1 \right) \\
A_4 &= \frac{1}{2\pi^2} \frac{1}{k_2^2 - q^2} L_1 \\
A_2 &= \frac{1}{4\pi^2} \left(\frac{k_2^2}{k_2^2 - q^2} L_1 - \frac{m^2}{k_2^2 - q^2} L_2 - 1 \right) \\
A_1 &= \frac{1}{4\pi^2} \left(\frac{k_2^2}{k_2^2 - q^2} L_1 + \frac{m^2}{k_2^2 - q^2} L_2 + 1 \right) \\
A_5 &= -A_4 - \frac{3}{\pi^2} k_2^2 \frac{d}{dk_2^2} \left(\frac{1}{k_2^2 - q^2} L_1 \right) \\
&\quad + \frac{3}{2\pi^2} k_2^4 \left(\frac{d}{dk_2^2} \right)^2 \left(\frac{1}{k_2^2 - q^2} L_1 \right) \\
&\quad + \frac{3}{4\pi^2} k_2^2 \frac{d}{dk_2^2} \left(\frac{1}{k_2^2 - q^2} L_2 \right) \\
&\quad + \frac{1}{2\pi^2} m^2 k_2^2 \left(\frac{d}{dk_2^2} \right)^2 \left(\frac{1}{k_2^2 - q^2} L_2 \right)
\end{aligned} \tag{2.13}$$

where

$$\begin{aligned}
L_1 &= -\rho \ln \frac{\rho+1}{\rho-1} + \beta \ln \frac{\beta+1}{\beta-1} \\
L_2 &= -\rho \ln^2 \frac{\rho+1}{\rho-1} + \beta \ln^2 \frac{\beta+1}{\beta-1} \\
\rho^2 &= 1 - 4m^2/q^2, \quad \beta^2 = 1 - 4m^2/k_2^2.
\end{aligned} \tag{2.14}$$

Note that the simple relationship between A_6 and A_2 in Eq. (2.13) is required by the Ward identity (2.7) which, when $k_1^2=0$, becomes

$$A_2 = k_1 \cdot k_2 A_6 = \frac{q^2 - k_2^2}{2} A_6. \tag{2.15}$$

If the limit $m^2 \rightarrow 0$ is taken in Eq. (2.13) the result is

$$\begin{aligned}
A_1 &= \frac{1}{4\pi^2} \left(\frac{k_2^2}{k_2^2 - q^2} \ln \frac{k_2^2}{q^2} + 1 \right) \\
A_2 &= \frac{1}{4\pi^2} \left(\frac{k_2^2}{k_2^2 - q^2} \ln \frac{k_2^2}{q^2} - 1 \right) \\
A_3 &= -A_6 = \frac{1}{2\pi^2} \frac{1}{k_2^2 - q^2} \left(\frac{k_2^2}{k_2^2 - q^2} \ln \frac{k_2^2}{q^2} - 1 \right).
\end{aligned} \tag{2.16}$$

While the Ward identity (2.7) does not determine A_5 in this limit, A_4 can be obtained from Eq. (2.8).

If instead the limit $k_2^2 \rightarrow 0$ is taken, with $m^2 > 0$, the result is

$$\begin{aligned}
A_6 &= -A_3 = \frac{1}{2\pi^2} \frac{1}{q^2} \left(1 + \frac{m^2}{q^2} \ln^2 \frac{\rho+1}{\rho-1} \right) \\
A_4 &= -A_5 = -\frac{1}{2\pi^2} \frac{1}{q^2} \left(2 - \rho \ln \frac{\rho+1}{\rho-1} \right).
\end{aligned} \tag{2.17}$$

$A_1 = -A_2$ can be obtained from the vector Ward identities and using Eq. (2.10) gives [21]

$$\begin{aligned}
T_{\mu\alpha\beta} &= A_6 q_\mu \epsilon_{\alpha\beta\sigma\delta} k_1^\sigma k_2^\delta + (A_4 + A_6) (\epsilon_{\mu\alpha\sigma\delta} k_1^\sigma k_2^\delta k_{2\beta} \\
&\quad - \epsilon_{\mu\beta\sigma\delta} k_1^\sigma k_2^\delta k_{2\alpha})
\end{aligned} \tag{2.18}$$

where A_4 and A_6 are given by Eq. (2.17). Note that the first term has the form of Eq. (2.9). This is consistent just because $k_1^2 = k_2^2 = 0, q^2 \neq 0$ is not possible in a symmetric momentum configuration. Also the anomaly is produced by the first term alone while, within the momentum configuration that we are discussing, each term separately satisfies the vector Ward identities.

When $k_2^2 \rightarrow 0$, with q^2 fixed, Eq. (2.16) gives

$$A_{1,2} \rightarrow \pm \frac{1}{4\pi^2}, \quad A_3 \rightarrow \frac{1}{2\pi^2} \frac{1}{q^2}. \tag{2.19}$$

That is, a pole appears in A_3 ($= -A_6$). If, instead, we integrate over spacelike values of q^2 , we obtain

$$\begin{aligned}
\int dq^2 A_3(q^2, k_2^2) f(q^2, k_2^2) &\xrightarrow[k_2^2 \rightarrow 0]{} \frac{1}{\pi} f(0, 0) \\
&= \int dq^2 \frac{1}{\pi} \delta(q^2) f(q^2, 0)
\end{aligned} \tag{2.20}$$

[provided $f(q^2, k_2^2)$ is regular at $q^2, k_2^2 = 0$].

The pole that appears in A_3 (and A_6) is the ‘‘anomaly pole’’ discussed by a number of authors [18–21]. The coefficient coincides with that of the anomaly and it is possible to give general arguments [18,19] that this pole is directly required by Eq. (2.12). The simplest way to see that this might be the case is to note that if $k_1^2 = k_2^2 = 0$ and A_4 and A_5 are not (sufficiently) singular the identities (2.7) and (2.8) reduce to the very simple form

$$A_3 = \frac{2}{q^2} A_1, \quad A_6 = \frac{2}{q^2} A_2. \tag{2.21}$$

Equation (2.11) then leads directly to Eq. (2.19). In fact, we will see below how the momentum routing of Fig. 1 that produces the ultraviolet anomaly (2.11) is also responsible for the numerator that accompanies the anomaly pole.

The amplitudes A_4 and A_5 will play very little role in our discussion. It is well known that these amplitudes do not contribute at $k_1^2 = k_2^2 = 0$ when $T_{\mu\alpha\beta}$ is contracted with physi-

cal polarization tensors. Our analysis will also be concerned with momentum configurations and components of $T_{\mu\alpha\beta}$ such that these amplitudes do not contribute. Note that Eq. (2.17) implies, and it is straightforward to check directly from Eq. (2.13), that the limits $m \rightarrow 0$ and $k_1^2, k_2^2 \rightarrow 0$ do not commute for A_4 and A_5 . A property that we will avoid in our analysis.

Finally we emphasize that if we keep only the pole terms in $T_{\mu\alpha\beta}$, as we will eventually do, then the vector Ward identities will necessarily be violated, for at least some momenta. As elaborated in [15] the Reggeon Ward identities that are necessary to avoid infrared divergences in Regge limit amplitudes depend on Ward identities being satisfied for all momenta. We will see below that when the Ward identities are satisfied only by a limited range of momenta, infrared divergences occur that, nevertheless, produce gauge-invariant amplitudes.

C. Interpretation

The results of the previous subsection extend straightforwardly to the case when there are gauge and flavor symmetries and $T_{\mu\alpha\beta}$ is a three-point amplitude for currents defined in terms of appropriate combinations of fermion fields. The anomaly in Eq. (2.12) is then a number determined by adding all contributing triangle diagrams. Most importantly, as is very well known, the ultraviolet anomaly in all (flavored) axial current Ward identities remains unchanged as gauge field interactions are included [25]. As a result, the general arguments alluded to above [18,19] [and more directly the identities (2.21)] determine that a pole with coefficient given by the anomaly is always present in the special kinematic configuration $k_1^2 = k_2^2 = m^2 = 0$. As first argued by 't Hooft [17], if there is confinement and there are no physical massless fermions, this pole has to be reproduced by a Goldstone boson pole. As we will discuss in the next section, this will provide the basis for our use of the chiral flavor anomaly to extract ‘‘infinite momentum’’ pion couplings to physical current components that produce scattering amplitudes. For the U(1) anomaly there will be no Goldstone boson pole but instead the δ function (2.20), produced by the integration of the anomaly pole over q^2 , will contribute in an essential manner to infinite momentum amplitudes.

To interpret the pole in Eq. (2.1) in terms of Landau singularities we note the following. The expressions for the A_i given above demonstrate that, when a fermion mass m is present, only two-particle normal thresholds are present in each invariant channel. These thresholds are responsible for the $\ln q^2$ and $\ln k_2^2$ factors that are present in Eq. (2.17). The pole at $q^2 = k_2^2$, which is superficially present in each of the

A_i , cancels when the logarithms have their physical sheet values. On unphysical sheets of the logarithms a pole is present and corresponds to the triangle Landau singularity. When $k_2^2 \rightarrow 0$ followed by $q^2 \rightarrow 0$ the physical sheet thresholds coincide at the point of interest and the unphysical sheet singularity is able to enhance the thresholds.

The simplest example of this last discussion is provided by Eq. (2.17) which gives

$$A_6(q^2, m^2) \xrightarrow{q^2 \rightarrow 0} \frac{1}{2\pi^2} \frac{1}{q^2} \left(1 + \frac{m^2}{q^2} \ln^2 \right) \times \left[1 + \left(\frac{-q^2}{m^2} \right)^{1/2} + \dots \right] \rightarrow \infty \quad (2.22)$$

$$A_4(q^2, m^2) \xrightarrow{q^2 \rightarrow 0} \frac{1}{2\pi^2} \frac{1}{q^2} \left(2 - \rho \ln \left[1 + \frac{2}{\rho} + \dots \right] \right) \rightarrow \infty$$

and so, for $m^2 \neq 0$, the pole is absent. The only finite q^2 singularity in either amplitude is the threshold at $q^2 = 4m^2$. If we continue around this threshold then $\rho \rightarrow -\rho$ and so

$$\ln \frac{\rho+1}{\rho-1} \rightarrow \pi i - \ln \frac{\rho+1}{\rho-1} \quad (2.23)$$

and the pole at $q^2 = 0$ is present. It is present on the physical sheet only at $m^2 = k_1^2 = k_2^2 = 0$.

We conclude that the Goldstone boson pole appears, in very special kinematics, because an unphysical singularity enters the edge of the physical region in the massless limit. It occurs in A_3 (and A_6), and not in the other A_i , because the unphysical singularity is a double pole rather than a single pole. It would be interesting to determine more explicitly how this feature relates to the momentum routing ambiguity associated with the anomaly.

D. Internal momentum analysis

In the next section we will want to derive anomaly pole couplings from the reduction of more complicated diagrams to triangle diagrams and also to separate the anomaly pole from the ultraviolet anomaly contribution. For these purposes it is important to determine the internal momenta p in Eq. (2.1) that generate the pole. We will see that light-cone momenta play a crucial role. Note that an external light-cone momentum is necessarily involved since if $k_1^2 = k_2^2 = q^2 = 0$ then, necessarily, $k_1 \parallel k_2 \parallel k_+$ where k_+ is lightlike. We first consider reaching the $q^2 = 0$ limit via the momentum configuration

$$k_1 = (k_+ / \sqrt{2}, k_+ / \sqrt{2}, 0, 0) \equiv k_1^+ = k_{1-} = k_+, \quad k_1^- = 0, \quad k_{1\perp} = 0 \quad (2.24)$$

$$k_2 = (-k_- / \sqrt{2}, k_- / \sqrt{2}, 0, 0) \equiv k_2^+ = 0, \quad k_2^- = k_{2+} = -k_-, \quad k_{2\perp} = 0$$

in which $k_1^2 = k_2^2 = 0$ and $q^2 = -2k_+k_-$.

We will shortly understand the anomaly pole contribution to Eq. (2.1) as produced by external momentum numerator factors together with a pole produced (by the denominators) in a part of the integration region that includes zero internal momentum. At first sight, Eq. (2.24) is not a very sensible configuration to discuss. If we consider the pole contribution of A_3 to T_{32-} , for example, this has the form

$$T_{23-} = -\epsilon_{\sigma\delta 23} \frac{k_1^\sigma k_2^\delta k_{1-}}{2\pi^2 q^2} = -\frac{k_+^2 k_-}{2\pi^2 q^2} = \frac{k_+}{4\pi^2} \quad (2.25)$$

and so there is no divergence as $q^2 \rightarrow 0$. At best we can obtain a finite contribution by taking $q^2 \sim k_- \rightarrow 0$, with k_+ kept finite. As a consequence, in the momentum configuration (2.24), the anomaly pole contribution cannot be distinguished from other nonsingular contributions. However, for our initial goal of obtaining a simple understanding of the origin of the denominator pole the momentum configuration (2.24) will be very useful. (Indeed, it will play a key role throughout the paper.)

If we drop the numerator terms in Eq. (2.1) and keep only the k_+ and k_- dependence we obtain

$$I(k_+, k_-, m^2) = I(q^2, m^2) = \int dp_+ dp_- d^2 p_\perp [2p_+(p_- - k_-) - p_\perp^2 - m^2 + i\epsilon]^{-1} \\ \times [2(p_+ - k_+)(p_- - k_-) - p_\perp^2 - m^2 + i\epsilon]^{-1} [2(p_+ - k_+)p_- - p_\perp^2 - m^2 + i\epsilon]^{-1}. \quad (2.26)$$

We will find that $I(q^2, m^2)$ is finite as $\epsilon \rightarrow 0$ only when $m^2 \neq 0$. This is not surprising since $I(q^2, m^2)$ is closely related to A_4 and A_6 , as given by Eq. (2.17). As we already noted above, the $k_1^2, k_2^2 \rightarrow 0$ limit commutes with the massless limit for A_6 , but not for A_4 . As a result, we expect that for part of $I(q^2, m^2)$ the limit $m^2 \rightarrow 0$ will not exist. [Of course, the numerator terms in Eq. (2.1) will play a central role in determining the nature of the divergence that occurs.] However, the pole term we are looking for appears, with the same (anomaly) coefficient, in both kinematic terms in Eq. (2.18) as $m^2 \rightarrow 0$. We therefore anticipate that the momentum region generating it will be unambiguous in this limit.

We will first evaluate $I(q^2, m^2)$ exactly. After we determine the origin of the pole we will give a more direct argument to locate the contributing momentum region. We begin by making the (scaling) change of variables

$$p_+ = x_+ k_+, \quad p_- = x_- k_-, \\ p_\perp = (k_+ k_-)^{1/2} x_\perp \quad (2.27)$$

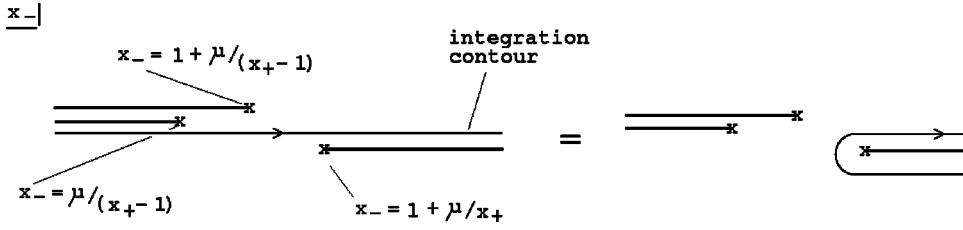
and also write $m^2 - i\epsilon = 2k_+ k_- \mu = -q^2 \mu$. If we carry out the angular x_\perp integration (which gives a factor of 2π) and write $y = x_\perp^2/2$ we then have

$$I(q^2, m^2) = \frac{\pi}{4q^2} I(\mu) = \frac{\pi}{4q^2} \int_{-\infty}^{+\infty} dx_+ \int_{-\infty}^{+\infty} dx_- \int_0^{+\infty} dy \\ \times \frac{1}{[(x_- - 1)x_+ - y - \mu][(x_- - 1)(x_+ - 1) - y - \mu][x_-(x_+ - 1) - y - \mu]}. \quad (2.28)$$

The propagators can be separated via partial fractions and the y integration can then be carried out to give

$$I(\mu) = \int_{-\infty}^{+\infty} dx_+ \int_{-\infty}^{+\infty} dx_- \frac{1}{(x_- - 1)(x_- - x_+)} \ln[(x_- - 1)x_+ - \mu] - \frac{1}{(x_+ - 1)(x_- - x_+)} \\ \times \ln[x_-(x_+ - 1) - \mu] + \frac{1}{(x_- - 1)(x_+ - 1)} \ln[(x_- - 1)(x_+ - 1) - \mu]. \quad (2.29)$$

We can evaluate Eq. (2.29) by contour integration in the x_- plane as follows. The three logarithmic branch points are on the same side of the x_- integration and the contour can be closed to zero unless $1 > x_+ > 0$. [Note that if the numerators of Eq. (2.1) were present then we could not close the contour without obtaining a contribution from the large x_- region.] When $1 > x_+ > 0$ the logarithmic branch cuts lie as illustrated in Fig. 2.


 FIG. 2. The x_- plane ($\mu = [m^2 - i\epsilon]/q^2$).

In this case, the contour can be closed around the one branch cut, as illustrated, and $I(\mu)$ is then given as an integral over just this discontinuity, i.e.

$$\begin{aligned} I(\mu) &= 2\pi i \int_0^1 dx_+ \int_{1+\mu/x_+}^{\infty} dx_- \frac{1}{(x_- - 1)(x_- - x_+)} \\ &= 2\pi i \int_0^1 dx_+ \frac{1}{1-x_+} \ln[1 + x_+(1-x_+)/\mu] \end{aligned} \quad (2.30)$$

which an integration by parts allows us to rewrite as

$$\begin{aligned} I(\mu) &= 2\pi i \int_0^1 dx_+ \ln[1-x_+] \frac{1-2x_+}{\mu+x_+(1-x_+)} \\ &\xrightarrow{\mu \rightarrow 0} 2\pi i \int_0^1 dx_+ \ln[1-x_+] \left[\frac{1}{x_+} - \frac{1}{(1-x_+)} \right]. \end{aligned} \quad (2.31)$$

The first term in Eq. (2.31) is finite while the second one has a logarithmic divergence of the kind we expected to find. As we discussed, we expect this divergence to be modified by, and to be dependent on, the numerator terms that we are presently ignoring. The first term we expect to be closely related to the anomaly pole term. If we consider the behavior of the integrands of both terms near $x_+ = 0$ then we note that the first term has a constant term in its Taylor expansion while the second does not. If we extract this term as a piece that is independent of how we handle the divergence of the second term we obtain

$$I(\mu) = 2\pi i \int_0^1 dx_+ [1 + O(x_+)] = 2\pi i + \dots \quad (2.32)$$

giving

$$I(q^2, m^2) \xrightarrow{\mu \rightarrow 0} \frac{\pi^2 i}{2q^2} + \dots \quad (2.33)$$

If an additional function $R(p_+, p_-, p_\perp)$ (produced by propagator numerators, for example) were present in the integrand of $I(q^2, m^2)$ then, if we again use the limit $k_- \rightarrow 0$ to obtain $q^2 \rightarrow 0$, the pole residue would simply contain an additional factor of $R(0,0,0)$.

Note that if we cut off the x_- integration at $x_- = \lambda_-$ we obtain an extra contribution to $I(0)$ of the form

$$\begin{aligned} I(0) &= 2\pi i \int_0^1 dx_+ \frac{1}{1-x_+} \ln \left[\frac{\lambda_- - x_+}{\lambda_- - 1} \right] \\ &= 2\pi i \int_0^1 dx_+ \ln[1-x_+] \left[\frac{1}{\lambda_- - x_+} - \frac{1}{\lambda_- - 1} \right] \end{aligned} \quad (2.34)$$

in which the integrand has no constant term in its expansion around $x_+ = 0$ and so, in this sense, does not modify the anomaly term extracted in Eq. (2.32). Therefore the anomaly term originates close to the lower end point for the x_- integration (i.e. $x_- = p_-/k_- \sim 1$) and is, indeed, independent of how we treat the large x_- region.

That the integration by parts, to obtain Eq. (2.31), is necessary to clearly expose the anomaly term is a consequence of the contour integration we used. We can extract the same term more directly from $I(q^2, m^2)$ as follows. First we write

$$\int_0^{+\infty} \frac{dy}{[(x_- - 1)(x_+ - 1) - y - \mu]} \xrightarrow{\mu \rightarrow 0} \ln(x_+ - 1) + \dots \quad (2.35)$$

giving, if we undo the scaling of x_- ,

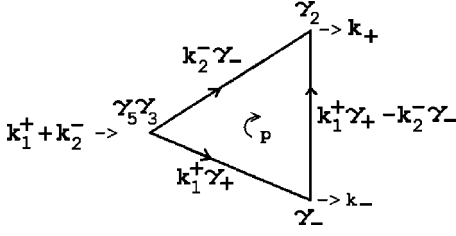
$$I(q^2, m^2) \rightarrow \frac{\pi}{8k_+} \int_0^1 dx_+ \ln(x_+ - 1) \int_{-\infty}^{+\infty} dp_- \frac{1}{[(p_- - k_-)x_+ - m^2/2k_+][p_-(x_+ - 1) - m^2/2k_+]} + \dots \quad (2.36)$$

We can then close the p_- contour around the second pole to obtain, in the limit $m^2 \rightarrow 0$,

$$\begin{aligned} I(q^2) &= \frac{\pi^2 i}{4k_+} \left(\int_0^1 dx_+ \frac{\ln(1-x_+)}{k_- x_+} \right) + \dots \\ &= \frac{\pi^2 i}{2q^2} + \dots \end{aligned} \quad (2.37)$$

which reproduces Eq. (2.31), and hence Eq. (2.33), directly.

Note that the denominator $k_- x_+$ in Eq. (2.37) is provided by the propagator that carries only the k_- external momentum. The factors k_-^{-1} and x_+^{-1} represent the separate ‘‘particle’’ and ‘‘antiparticle’’ poles of this propagator and both contribute in an essential manner. k_-^{-1} produces the $(q^2)^{-1}$ pole in the final result. The residue of the pole at $x_+ = 0$,

FIG. 3. Vertices and propagator numerators for $\Gamma_{32-}(k_+, k_-)$.

multiplied by $\ln(1-x_+)$ [which is the integrated propagator contribution obtained from Eq. (2.35)], is integrated to produce the final anomaly coefficient. That both particle and antiparticle poles contribute to the anomaly pole is a very important point that we will elaborate on shortly.

To determine that Eq. (2.33) is indeed the anomaly coefficient that we want we must reintroduce the propagator numerators, that we have so far neglected, and evaluate them at zero internal momentum. In the configuration (2.24) the external momentum numerators contribute the combination of lightlike momenta and γ matrices shown in Fig. 3. The corresponding contribution to $\Gamma_{32-}(k_+, k_-)$ is

$$\begin{aligned} & \text{Tr}\{\gamma_5 \gamma_3 [k_2 \cdot \gamma] \gamma_2 [k_1 \cdot \gamma] \gamma_- [(k_1 - k_2) \cdot \gamma]\} \\ &= \text{Tr}\{\gamma_5 \gamma_3 [k_2^- \gamma_-] \gamma_2 [k_1^+ \gamma_+ - k_2^- \gamma_-] \gamma_- [k_1^+ \gamma_+]\} \\ &= \text{Tr}\{\gamma_5 \gamma_3 \gamma_- \gamma_2 \gamma_+ \gamma_- \gamma_+\} k_+^2 k_- \\ &= -2 \text{Tr}\{\gamma_5 \gamma_3 \gamma_2 \gamma_- \gamma_+\} k_+^2 k_-. \end{aligned} \quad (2.38)$$

The well-known identity for a product of three orthogonal γ matrices

$$\gamma_\alpha \gamma_\beta \gamma_\lambda = g_{\alpha\beta} \gamma_\lambda + g_{\beta\lambda} \gamma_\alpha - g_{\alpha\lambda} \gamma_\beta + i \epsilon_{\mu\alpha\beta\gamma} \gamma^\mu \gamma_5 \quad (2.39)$$

then gives

$$\begin{aligned} -4 \text{Tr}\{i \gamma_5^2 + \gamma_5 \gamma_2 \gamma_3\} k_+^2 k_- &= 4i \text{Tr}\{\gamma_5^2\} k_+^2 k_- \\ &= 16i k_+^2 k_-. \end{aligned} \quad (2.40)$$

Combined with Eq. (2.33), this gives the desired contribution of the anomaly pole [after taking into account the factor of $1/(2\pi)^4$ in the original integral (2.1)].

If we return to the original momenta we see from Eqs. (2.35)–(2.37) that the relevant integration region for the anomaly pole is

$$(i) p_\perp^2 \lesssim q^2 \quad (ii) 0 \leq p_+ \leq k_+ \quad (iii) p_- \sim k_- \rightarrow 0 \quad (2.41)$$

and that any additional factors in the integrand (besides the propagator denominators) are to be evaluated at zero internal momentum. The surviving external light-cone momentum then flows directly around two of the three internal propagators. This will be very important in the next section.

In the following, we will use manipulations analogous to Eqs. (2.38) and (2.40), in which the numerators carrying the limiting momentum configuration are combined, to determine whether the anomaly is present in diagrams. However, as we noted above, the anomaly pole terms are not actually singular in the limiting momentum configuration we have discussed. To consistently isolate anomaly pole contributions to $\Gamma_{\mu\alpha\beta}$ it is necessary to work in a kinematical configuration where singular contributions are obtained. This is the case if an additional external transverse momentum q_\perp is part of the limiting momentum configuration, such that $q_\perp^2 \sim q^2$, while the corresponding propagator numerator provides a factor that is $O(q_\perp)$ and vanishes more slowly than q^2 . We will, nevertheless, be able to apply the above analysis by exploiting the Lorentz invariance properties of the internal momentum integration.

E. Frame dependence of the anomaly numerator

A second momentum configuration that can be used to approach $q^2=0$ is

$$\begin{aligned} k_1 &= (k/\sqrt{2}, k/\sqrt{2}, 0, 0) \equiv k_1^+ = k, \quad k_{1-} = 0, \quad k_\perp = 0 \\ k_2 &= (-k/\sqrt{2}, -k \cos \theta/\sqrt{2}, 0, -k \sin \theta/\sqrt{2}) \\ &\underset{\theta \rightarrow 0}{\sim} -k_1 - (0, 0, k \theta/\sqrt{2}, 0) = -k_1 - (0, 0, q, 0) \end{aligned} \quad (2.42)$$

where

$$q^2 = (k_1 + k_2)^2 \underset{\theta \rightarrow 0}{\sim} . \quad (2.43)$$

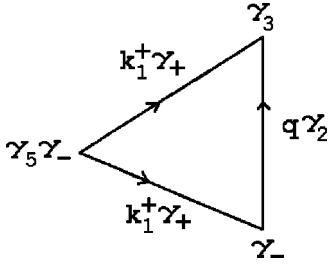
In the configuration (2.42), we obtain the largest numerator if we consider the anomaly contribution of A_3 to T_{--3} . This has the form

$$T_{--3} = \epsilon_{\sigma\delta-3} \frac{k_1^\sigma k_2^\delta k_{1-}}{q^2} = \frac{k^2 [k \theta / \sqrt{2}]}{q^2} \underset{\theta \rightarrow 0}{\sim} \sqrt{\frac{2k}{\theta}} \quad (2.44)$$

and so a divergence is present.

In the limit $q \rightarrow 0$, the external momentum flow and γ -matrix couplings are now as shown in Fig. 4. Essentially the same calculation as Eqs. (2.38) and (2.40) gives the numerator in Eq. (2.44) directly from the external momentum propagator numerators. (Note that the propagator that carries zero momentum in the limiting configuration is now that corresponding to the vertical line in Fig. 4.) It remains, therefore, to understand the anomaly pole as arising from an internal zero momentum configuration.

Since all invariants remain unchanged it must, of course, be possible to obtain Eq. (2.42) from Eq. (2.24) via a Lorentz transformation. This can be done as follows. We first set


 FIG. 4. Vertices and propagator numerators for T_{--3} .

$k_+ = k_- = q$ (which can be done trivially via a Lorentz transformation to the “center of mass frame”). We then apply a boost $a_y(\zeta)$ to obtain

$$\begin{aligned} k_1 &\rightarrow \left(\frac{q \cosh \zeta}{\sqrt{2}}, \frac{q}{\sqrt{2}}, \frac{q \sinh \zeta}{\sqrt{2}}, 0 \right) \\ k_2 &\rightarrow \left(\frac{q \cosh \zeta}{\sqrt{2}}, -\frac{q}{\sqrt{2}}, \frac{q \sinh \zeta}{\sqrt{2}}, 0 \right) \\ &= k_1 - (0, \sqrt{2}q, 0, 0) \end{aligned} \quad (2.45)$$

which, if $q \cosh \zeta = k$ is kept finite as $q \rightarrow 0$, differs from Eq. (2.42) only by a rotation.

If we consider Eq. (2.1) directly in the momentum configuration (2.42), the numerator contribution giving Eq. (2.44) will be multiplied by a denominator integral that is a Lorentz invariant. If the reverse Lorentz transformation to that giving Eq. (2.42) from Eq. (2.24) is applied to the momentum integration variables then $I(q^2, 0)$, as given by Eq. (2.28), will appear and the above analysis can be used to extract the anomaly pole, with Eq. (2.42) now appearing as the limiting momentum configuration. This implies, of course, that the limit $q^2 \rightarrow 0$ is provided by an internal momentum configuration that is reached by an infinite boost from the original zero momentum region.

We can further enhance the anomaly numerator if we instead apply $a_y(\zeta)$ directly to Eq. (2.24), but now let $q^2 \rightarrow 0$ by taking $k_- \rightarrow 0$. This gives

$$\begin{aligned} k_1 &\rightarrow \left(\frac{k_+ \cosh \zeta}{\sqrt{2}}, \frac{k_+}{\sqrt{2}}, \frac{k_+ \sinh \zeta}{\sqrt{2}}, 0 \right) \\ k_2 &\rightarrow \left(\frac{k_- \cosh \zeta}{\sqrt{2}}, -\frac{k_-}{\sqrt{2}}, \frac{k_- \sinh \zeta}{\sqrt{2}}, 0 \right) \end{aligned} \quad (2.46)$$

and so, for example, T_{23-} (defined with respect to the axes of the new frame) is given by

$$\begin{aligned} T_{23-} &\sim \epsilon_{\sigma\delta 23} \frac{k_1^\sigma k_2^\delta k_{1-}}{q^2} \\ &\sim \frac{[-k_+ k_- \cosh \zeta] k_+ \cosh \zeta}{\sqrt{2} q^2}. \end{aligned} \quad (2.47)$$

Now, if we let $k_- \rightarrow 0$ and take $\cosh \zeta \rightarrow \infty$ such that $k_- \cosh \zeta$ remains finite, the numerator in Eq. (2.47) $\rightarrow \infty$ while $q^2 \rightarrow 0$ and most importantly (as we discuss in the next subsection) that part of the numerator contained in square brackets remains finite. This demonstrates that the anomaly pole can have a finite coupling to infinite momentum states. [It is, of course, crucial for the enhancement (2.47) that the tensor component discussed is defined with respect to the axes of the new frame.]

It will be important in succeeding sections that both the component of $T_{\mu\alpha\beta}$ that dominates and the zero momentum line involved, depend on how the anomaly pole limit is approached (or, equivalently, the Lorentz frame involved). This is because our analysis of anomaly contributions in high-energy scattering is not Lorentz invariant, but rather we combine contributions that are (initially calculated) in different finite and infinite momentum frames.

As noted in [18], if we consider the helicities of the internal massless fermions producing the anomaly pole numerator we find that the fermion that carries zero momentum must effectively flip its helicity. Equivalently, it must reverse its particle-antiparticle identification. The vertex at one end of the propagator must be that for production of a particle while, simultaneously, that at the other end describes the production of the antiparticle. This is possible just because, as we discussed above, both particle and antiparticle poles contribute to a divergence that occurs when the propagator carries zero momentum. This process is an integral part of the formation of a pion pole.

The pion scattering amplitude that we derive in the next section will also contain a zero momentum propagator [within a U(1) anomaly interaction] which describes a physical zero momentum transition. If this process, and that producing the pion pole, are to be interpreted as a physical processes the Dirac sea must be shifted at the second vertex relative to the first. The production of the antiparticle has to be reinterpreted as production of a state that fills a hole in the sea, i.e. the absorption of an antiparticle. That is to say, there must be spectral flow of the Dirac sea during the interaction. In a field-theoretic path integral language, this phenomenon is what produces a “chirality transition” due to a topological background gauge field. However, in our discussion there is no implication that a topological background field is involved.

We also note that the part of our calculation of the “anomaly pole” in the above that involved only the denominators could equally well be applied to the calculation [26] of a gluon triangle (involving an effective vertex) that appears in the coupling of a Reggeized gluon to on-shell gluons. This coupling need not satisfy a gauge invariance Ward identity. Of course, the ϵ -tensor structure of the anomaly that is due to the fermionic numerators will not occur. However, a particle-antiparticle transition, via a zero momentum propagator, can be responsible for the helicity transition that occurs.

The ultraviolet anomaly is well known to originate from the region

$$p_+ \sim p_- \sim p_\perp \rightarrow \infty. \quad (2.48)$$

Therefore, in principle, we can keep the anomaly pole in $T_{\mu\alpha\beta}$ while dropping the ultraviolet anomaly if we integrate only over the momentum region (2.41). Isolating the anomaly pole from the ultraviolet anomaly will be an important part of our analysis in the following. While we can suppose that, as a matter of principle, we are restricting the integration region, in practice we will simply use an anomaly pole coupling as discussed in the following subsection. This violates full gauge invariance but, as we discuss, if we keep only the anomaly pole term and restrict our analysis to $k_1^2 = k_2^2 = 0, q^2 \sim 0$, we will keep the partial gauge invariance that is sufficient to produce gauge-invariant amplitudes. Nevertheless, the loss of full gauge invariance plays a crucial role in generating the transverse momentum infrared divergences that are the cornerstone of our confinement dynamics. By manipulating the relative contributions of the anomaly pole and the ultraviolet anomaly we will effectively be regulating the relative ultraviolet and infrared spectral flow.

F. The pole residue as a Goldstone boson coupling

A major question is whether we can use the identification of the anomaly pole as a Goldstone boson pole to obtain information about the interactions of physical Goldstone bosons. If we keep just the anomaly pole contributions of A_3 and A_6 to $T_{\mu\alpha\beta}$ we can write

$$T_{\mu\alpha\beta}(k_1, k_2) = -\frac{1}{2\pi^2} \frac{(\epsilon_{\delta\sigma\alpha\mu} k_{1\beta} - \epsilon_{\delta\sigma\beta\mu} k_{2\alpha}) k_1^\delta k_2^\sigma}{(k_1 + k_2)^2} + \dots \quad (2.49)$$

This expression does not satisfy the vector Ward identities and does not have the axial current anomaly. According to the above discussion, it is nevertheless obtained if we keep only the integration region (2.41) in Eq. (2.1), together with the momentum dependence of propagator numerators given by the external momenta.

When $k_1^2 = k_2^2 = 0$, we can use the identity (2.10) to obtain [what is essentially Eq. (2.18) with $m^2 \rightarrow 0$]

$$T_{\mu\alpha\beta}(k_1, k_2) = -\frac{1}{2\pi^2} \frac{[-\epsilon_{\delta\sigma\alpha\beta} [k_1 + k_2]_\mu + (\epsilon_{\delta\sigma\beta\mu} k_{1\alpha} - \epsilon_{\delta\sigma\alpha\mu} k_{2\beta})] k_1^\delta k_2^\sigma}{(k_1 + k_2)^2} + \dots \quad (2.50)$$

where the additional omitted terms are those that are less singular as $q^2 = (k_1 + k_2)^2 \rightarrow 0$. [Note that to justify omitting these terms it is crucial that we consider a component in which there is a singularity at $q^2 = 0$ and the numerator does not cancel the denominator singularity, as in (2.25).] Each term in Eq. (2.50) separately satisfies the vector Ward identities (for momenta which satisfy $k_1^2 = k_2^2 = 0$) but only the first term has the appropriate factorized form to provide a pion pole coupled to the axial current A_μ . The second term corresponds to the A_4 and A_5 contributions in Eq. (2.3) which we anticipated would not contribute to the tensor components that would appear in our discussion. Therefore, we might expect that we can use

$$T_{\mu\alpha\beta}(k_1, k_2) = \frac{1}{2\pi^2} \frac{[k_1 + k_2]_\mu \epsilon_{\delta\sigma\alpha\beta} k_1^\delta k_2^\sigma}{(k_1 + k_2)^2} + \dots \quad (2.51)$$

to obtain physical pion pole couplings, anticipating that $[k_1 + k_2]_\mu$ provides the coupling to the axial current A_μ while the factor $\epsilon_{\delta\sigma\alpha\beta} k_1^\delta k_2^\sigma$ provides the coupling to currents V_α and V_β . [In a general current vertex the $1/2\pi^2$ in Eq. (2.51) will be replaced by the appropriate anomaly coefficient.] Equation (2.51) not only satisfies the vector Ward identities but also produces the anomaly in the axial current. Remarkably, perhaps, we have obtained these properties from Eq. (2.49) simply by restricting to the momentum region

$$k_1^2 = k_2^2 = 0, \quad q^2 \rightarrow 0 \quad (2.52)$$

and asking for a factorizable pole residue. Therefore, if we restrict our discussion to the region (2.52) [and to components of $T_{\mu\alpha\beta}$ to which the second term in Eq. (2.50) does not give a leading contribution] all desired, factorization, gauge invariance and anomalous divergence properties are contained in Eq. (2.51).

While it is well known that Eq. (2.51) describes well the decay of a physical (massive) pion into physical photons there is, not surprisingly, an obvious problem with attempting to use it to discuss the coupling of a pion to dynamical gluon currents. It is crucial for our infrared anomaly analysis that the ‘‘pion’’ is massless. In this case the ‘‘pion pole’’ appears only in the $q^2 \rightarrow 0$ limit in which $k_1 \parallel k_2 \parallel k_+$ where k_+ is lightlike. Because of the ϵ tensor, the numerator in Eq. (2.51) then vanishes in any finite momentum configuration—as we have seen explicitly above. In general, if the limiting configuration is approached via a vanishing spacelike momentum q and k_+ is the nonvanishing component of k then, at best,

$$\epsilon_{\delta\sigma\alpha\beta} k_1^\delta k_2^\sigma \sim k_+ q \quad (2.53)$$

which, of course, still vanishes as $q \rightarrow 0$. The fundamental reason for this is that Eq. (2.51) is antisymmetric in k_1 and k_2 and, because of Bose symmetry, can only describe the contribution of antisymmetric momentum configurations of the kind we have discussed. For consistency, it must vanish at the symmetric point where $k_1^2 = k_2^2 = q^2 = 0$. The conclusion is, clearly, that we cannot obtain a finite coupling as $q^2 \rightarrow 0$ and the limit onto the (massless) pion mass shell is

taken. Therefore, the anomaly provides no information about physical, finite momentum, massless pion-gluon interactions.

However, we see from Eq. (2.47) that if we go to an “infinite momentum frame” we can keep components of q finite, even though $q^2 \rightarrow 0$ and the ratio q/k_+ goes to zero. If we use Eq. (2.51), instead of Eq. (2.47), to evaluate T_{23-} in this frame, we obtain

$$T_{23-} \sim \epsilon_{\sigma\delta 3} \frac{k_1^\sigma k_2^\delta k_{12}}{q^2} \sim \frac{[-k_+ k_- (\sinh \zeta)] k_+ \sinh \zeta}{\sqrt{2} q^2} \quad (2.54)$$

which, not surprisingly, gives the same leading result as Eq. (2.47). [Note that the second term in Eq. (2.50) gives a non-leading contribution.] The “infinite momentum” pion coupling is now given as

$$\epsilon_{\sigma\delta 3} k_1^\sigma k_2^\delta \sim [k_+ k_- \sinh \zeta] \quad (2.55)$$

which, as we noted above, is finite if $k_- \rightarrow 0$ with $k_- \cosh \zeta$ kept finite. We conclude that, although the anomaly provides no information about finite momentum gluon couplings, it can potentially provide information about the “wee-gluon,” or “wee-parton” couplings of the infinite momentum pion. We will discuss such couplings in the next section. We will find that the current component involved cannot be that of a simple local current but must itself originate from a nonlocal interaction that produces an effective local interaction at infinite momentum.

III. BUILDING COLOR SUPERCONDUCTING PION AMPLITUDES

A. The gluon and quark spectrum

When the gauge symmetry of QCD is spontaneously broken from SU(3) to SU(2) the resulting theory is commonly called “color superconducting QCD.” Our eventual goal is to give a detailed construction of high-energy scattering amplitudes (for Goldstone bosons) in color superconducting QCD and then to discuss the restoration of the full gauge symmetry using Reggeon field theory. In this paper we want to concentrate on how the kinematical and dynamical properties of the chiral flavor and U(1) anomalies discussed in the previous section combine with transverse momentum infrared divergences to produce such amplitudes. For this purpose we will use only general properties of the gluon and quark spectrum, which we now discuss, and will make only qualitative comments about color and color factors.

Some number of quark flavors will be present, which we will not specify since we will not give them distinct masses. The symmetry breaking could be due to the expectation value of a complex color triplet scalar field, with Yukawa couplings generating a mass for SU(2) singlet quarks. Alternatively, and perhaps preferably, since the scalar field itself plays no role in our discussion, the symmetry breaking could equally well be dynamical and due to a diquark condensate associated with the additional chiral symmetry breaking dis-

cussed below. Independently of the nature of the symmetry breaking, the complete structure of the broken gauge group, i.e. all the interactions of massless and massive gluons amongst themselves together with their interactions with massless and massive quarks, will be important.

The gluon spectrum consists of a massless SU(2) triplet, two massive SU(2) doublets with mass $\sim M_C$, and a massive singlet with mass M_C . The quark spectrum consists of a massless SU(2) doublet and a massive singlet for each flavor, with mass $m_C \sim M_C$. Because of the equivalence of quark and antiquark color representations, there is an extended chiral symmetry [22]. In particular, SU(2) color singlet axial currents can be formed from pairs of quark fields and pairs of antiquark fields, in addition to the usual quark-antiquark currents. We will generically refer to the SU(2) singlet quark-antiquark Goldstone bosons associated with chiral symmetry breaking as pions and will refer to the singlet quark-quark Goldstone bosons as nucleons.

We will be considering infrared divergences due to both the massless quarks and the massless gluons. To discuss these divergences we should, initially, invoke a second symmetry-breaking mechanism to give all quarks and gluons masses. A second complex triplet scalar could be used for this purpose or the symmetry breaking could again be dynamical. We simply assume that there is an initial mass M for the SU(2) gluons that is taken to zero and an SU(2) quark mass m that is also taken to zero. When $m \rightarrow 0$ the anomaly pole discussed in the last section, will be produced by massless quark loops. This will be our starting point. When the gluon mass $M \rightarrow 0$ also, there will be an overall infrared divergence that will produce confinement and select the color zero amplitudes in which the anomaly pole becomes a pion or nucleon pole. As we will see, our analysis involves only on mass-shell states and gauge-invariant transverse momentum diagrams. The only breaking of gauge invariance in our discussion will be that associated with phase-space cutoffs in anomaly generating diagrams. As we implied in the previous section, gauge invariance will be preserved for those momenta involved in physical amplitudes.

B. Transverse momentum infrared divergences

Before discussing anomaly couplings we first summarize, briefly, the established properties of the gauge-invariant massless transverse momentum diagrams that will be involved. The overall infrared divergence we discuss in the following will be produced when these diagrams couple through anomaly generating effective interactions.

It is well known from perturbative calculations [4–9] that in gauge theories the Regge limit is described by transverse momentum diagrams. When all gluons and quarks have a mass there are no infrared divergences and high-order leading and next to leading log calculations show that these diagrams exponentiate (in momentum space) to produce Regge pole and Regge cut behavior. Both gluons and quarks lie on Regge trajectories, i.e. they “Reggeize.” Reggeization of the gluon corresponds to the exponentiation

$$\begin{aligned} \frac{s}{t-M^2} &\equiv \frac{1}{t-M^2} \int \frac{dJS^J}{(J-1)} \rightarrow \frac{s^{1-\Delta(t)}}{t-M^2} \\ &\equiv \frac{1}{t-M^2} \int \frac{dJS^J}{(J-1+\Delta(t))} \end{aligned} \quad (3.1)$$

where $1-\Delta(t)$ is the (massive) gluon Regge trajectory given (in the leading log approximation) by

$$\begin{aligned} \Delta(-Q^2) &= \frac{(Q^2+M^2)}{16\pi^2} \int \frac{d^2k_1}{k_1^2+M^2} \frac{d^2k_2}{k_2^2+M^2} \\ &\quad \times \delta^2(Q-k_1-k_2). \end{aligned} \quad (3.2)$$

As is illustrated by Eq. (3.1), momentum space exponentiation corresponds to power series summation in the J plane ($J = \text{complex angular momentum}$). We can further illustrate this by considering an amplitude for which the leading high-energy behavior is given by the Regge-cut corresponding to two Reggeized gluons. In this case the lowest-order result is (apart from a normalization factor)

$$\begin{aligned} A_0(J,t) &= \frac{1}{J-1} \int \frac{d^2k_1}{k_1^2+M^2} \frac{d^2k_2}{k_2^2+M^2} \\ &\quad \times \delta^2(Q-k_1-k_2) \end{aligned} \quad (3.3)$$

where $t=Q^2$. The momentum space exponentiation corre-

sponding to Reggeization of the gluons is now described by replacing the fixed pole at $J=1$ by the two-Reggeon propagator

$$\Gamma_2 = \frac{1}{J-1+\Delta(k_1^2)+\Delta(k_2^2)} \quad (3.4)$$

giving

$$\begin{aligned} A_0(J,t) \rightarrow A(J,t) &= \int \frac{d^2k_1}{k_1^2+M^2} \frac{d^2k_2}{k_2^2+M^2} \\ &\quad \times \frac{\delta^2(Q-k_1-k_2)}{J-1+\Delta(k_1^2)+\Delta(k_2^2)}. \end{aligned} \quad (3.5)$$

Further momentum space exponentiation is provided by Reggeon interactions that, in the J plane, simply iterate Eq. (3.5), which we identify as a ‘‘two-Reggeon state.’’ The form of the interaction depends on the t -channel color of the iterated Reggeon state, i.e. we can write [5] (imposing $k_1+k_2=k'_1+k'_2$)

$$\begin{aligned} \Gamma_{22}(k_1, k_2, k'_1, k'_2) &= a(k_1+k_2)^2 + bM^2 \\ &\quad - cR_{22}(k_1, k_2, k'_1, k'_2), \end{aligned} \quad (3.6)$$

where a , b and c are color factors (that include an overall normalization factor) and

$$R_{22}(k_1, k_2, k'_1, k'_2) = \frac{(k_1^2+M^2)(k_2'^2+M^2) + (k_2^2+M^2)(k_1'^2+M^2)}{(k_1-k_1')^2+M^2} + \frac{(k_1^2+M^2)(k_1'^2+M^2) + (k_2^2+M^2)(k_2'^2+M^2)}{(k_1-k_2')^2+M^2}. \quad (3.7)$$

The (massive) BFKL equation [4] is simply the color zero Reggeon ‘‘Bethe-Salpeter’’ equation obtained by iterating the Reggeon interaction Γ_{22} in Reggeon diagrams. Γ_{22} is not a Fredholm kernel and so the solution of the BFKL equation need not contain only Regge poles. Indeed, the BFKL Pomeron is generated from the large transverse momentum region and is a fixed cut. For our purposes, we will impose an upper transverse momentum cutoff and (ultimately) will utilize only the infrared properties of the BFKL equation.

In general, it can be shown [27] that the contributions of all logarithms (down to an arbitrary nonleading level) can be described by transverse momentum diagrams. Abstract S matrix results [1–3] on unitarity in the complex angular momentum plane (Reggeon unitarity) imply that the transverse momentum diagrams can be organized into an elaborate exponentiation phenomenon in which a complete set of Reggeon diagrams appears, involving all possible J -plane multi-Reggeon states. For our present purposes we require only a few infrared properties that existing calculations, combined with general arguments, imply are satisfied by the complete set of Reggeon diagrams (or, equivalently, the complete set of transverse momentum diagrams). A more extensive discussion can be found in [9].

When $M \rightarrow 0$ infrared divergences appear in both the Reggeon trajectories and the (integrated) Reggeon interactions. At first sight the divergence

$$\Delta(Q^2) \xrightarrow{M^2 \rightarrow 0} \ln M^2 \quad (3.8)$$

exponentiates to zero all Reggeon amplitudes via the Regge pole exponentiation (3.1). In the J plane this exponentiation of divergences is reflected in the vanishing of the Reggeon propagator (3.4), and all higher multi-Reggeon propagators. However, since divergences also appear in the Reggeon interactions, to discuss the $M \rightarrow 0$ limit in detail, it is advantageous to undo the Reggeon diagram organization and go back to transverse momentum diagrams. The Reggeon interactions and Reggeon trajectory contributions can be combined into ‘‘kernels’’ $K_N^I(\dots, k_i, \dots, k_j', \dots)$, where I denotes $SU(2)$ color. If the kernels are defined to include a transverse momentum conserving δ -function they are dimensionless (in transverse momentum) and describe the iteration of dimensionless lowest-order ‘‘multigluon transverse momentum states’’ T_N where

$$T_N = \frac{1}{J-1} \int \prod_{i=1}^N \frac{d^2 k_i}{k_i^2}. \quad (3.9)$$

For example,

$$\begin{aligned} & K_2^I(k_1, k_2, k'_1, k'_2) \\ &= \delta^2(k_1 + k_2 - k'_1 - k'_2) \\ & \times \left[\Gamma_{2,2}^I(k_1, k_2, k'_1, k'_2) + k_1^2 k_2^2 [\Delta(k_1^2) + \Delta(k_2^2)] \right. \\ & \left. \times \left[\frac{1}{2} \delta^2(k_1 - k'_1) + \frac{1}{2} \delta^2(k_1 - k'_2) \right] \right]. \quad (3.10) \end{aligned}$$

For simplicity we refer to T_N as a ‘‘multigluon state’’ in the following. In this context a multigluon state will always be the lowest-order transverse momentum diagram contributing to a multi-Reggeon state. As such, the multigluon state will carry the color and signature properties of the parent multi-Reggeon state. Note that gauge invariance (in the form of Reggeon Ward identities [15]) implies that the kernels K_N^I have zeros (when any k_i or k'_j vanishes) which, at fixed Q^2 , prevent the poles in the T_N from producing divergences. At fixed Q^2 , therefore, the divergences come only from the trajectory and interaction terms contained in the kernels.

When the t -channel color is nonzero the divergences produced by $\Gamma_{2,2}^I$ do not cancel those due to the $\Delta(k_i^2)$ terms in Eq. (3.10) and, in general, for a multigluon kernel with nonzero color, the interaction divergences do not cancel the trajectory divergences. As a result

$$\begin{aligned} T_N K_N^I &= \frac{1}{J-1} \int \prod_{i=1}^N \frac{d^2 k_i}{k_i^2} \\ & \times K_N^I(\dots, k_i, \dots, k'_j, \dots) \rightarrow \infty, \\ & Q^2, I \neq 0 \quad (3.11) \end{aligned}$$

and so the exponentiate of divergences due to Reggeization dominates and sends the sum of all diagrams in any colored channel to zero, as illustrated in Fig. 5. When $I=0$ and $Q^2 \neq 0$, the trajectory and interaction divergences do cancel. As a result there is no exponentiation of divergences. K_2^0 , as given by Eq. (3.10), is the familiar (massless) BFKL kernel and if there is no ultraviolet cutoff on the transverse momenta (as we will shortly impose) the iteration shown in Fig. 5 produces the BFKL Pomeron.

The disappearance of all colored multigluon states is not confinement since, in the color zero diagrams, the gluon poles in the states remain—even though there is a cancellation of divergences for $Q^2 \neq 0$. If the iterated diagrams are coupled gauge invariantly to scattering states then such couplings will also have the necessary zeros to make the complete amplitude finite at fixed Q^2 . This is the infrared finiteness property which is extensively exploited in BFKL applications. Nevertheless, at $Q^2=0$ a singularity remains that is associated with the multigluon states and whose exact nature depends on the behavior of the kernels as $Q^2 \rightarrow 0$.

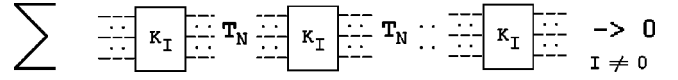


FIG. 5. Iteration of a massless gluon kernel.

Confinement could be produced if the $Q^2=0$ singularity can be absorbed into a ‘‘condensate,’’ as will be the case at the end of our analysis.¹

In leading-log calculations the infrared finiteness property of the dimensionless kernels leads directly to conformal scale invariance. In general nonleading log contributions the introduction of a scale for the gauge coupling destroys all scale-invariance properties. If, however, there is an infrared fixed point for the gauge coupling (as is the case when a large number of massless quarks are present) the scale invariance properties will still be present in the infrared region. In this paper we effectively assume the existence of such a fixed point. We will also, for the purposes of this paper, impose an upper cutoff on the transverse momenta. Infrared finiteness then implies that the kernels K_N^0 scale canonically as $Q^2 \rightarrow 0$ so that

$$\begin{aligned} & \int_{|k_i|^2, |k'_j|^2 < \lambda} \prod_i \frac{d^2 k_i}{k_i^2} \prod_j \frac{d^2 k'_j}{k'^2_j} K_N^0(k_1, \dots, k_N, k'_1, \dots, k'_N) \\ & \sim \int^{\lambda_\perp} \frac{dQ^2}{Q^2} \quad (3.12) \end{aligned}$$

where, as in the above, $Q = \sum k_i = \sum k'_j$. If Eq. (3.12) is obtained via the limit $M^2 \rightarrow 0$, this divergence would appear as a factor of $\ln[M^2/\lambda_\perp]$.

To understand the implications of this last divergence we formally rewrite Eq. (3.12), analogously to Eq. (3.11), as

$$(J-1)^2 T_N T'_N K_N^0 \quad (3.13)$$

and note that infrared finiteness implies firstly that $(J-1)T'_N K_N^0$ is finite when the k_i are finite and, also, that $(J-1)T_N K_N^0$ is finite when the k'_j are finite. Consequently, there are two contributions to the divergence in Eq. (3.12), depending on whether the Q^2 integration is performed as part of the integration over the k_i or as part of the integration over the k'_j . In the first case the divergence is obtained from the region $\{k_i \ll k'_j \forall i, j\}$, whereas in the second case it is the region $\{k'_j \ll k_i \forall i, j\}$. In effect, either the T_N or the T'_N integration produces the divergence, but not both.

If a color zero multigluon state is coupled without the Ward identity zero (involving the transverse momentum of the complete state) that is (normally) a consequence of gauge invariance, Eq. (3.12) is a potential source of an infrared

¹In effect, we will use the scale invariance properties of color SU(2) Reggeon diagrams, which generate all of the conformal symmetry properties of the BFKL Pomeron, only to generate a factorizing infrared condensate. We then build up the Regge pole nature of the Pomeron through the remaining, massive, part of the gauge group.

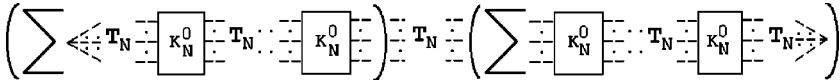


FIG. 6. Isolation of the divergence associated with T_N .

divergence. This will be the case for the anomaly couplings that we discuss below. It is important that as the kernel K_N^0 is iterated a divergence always occurs when $Q^2 \rightarrow 0$. The degree of divergence does not increase but rather, in an integral involving a product of many kernels, there is a distinct contribution from each T_N . The divergent T_N can then be isolated and the remaining integrations organized, in the complete set of diagrams, as illustrated in Fig. 6. It follows that the residue of the logarithmic divergence can be written in the factorized form

$$\frac{1}{J-1} \int \frac{dQ^2}{Q^2} \int \prod_i \frac{d^2 k_i}{k_i^2} \delta^2(Q - \sum k_i) \times |M_N^0(J, k_1, \dots, k_N, \lambda_\perp)|^2 \quad (3.14)$$

where M_N^0 is given by the sum of diagrams shown in Fig. 7.

In the following we will need to know the interaction between massless multigluon states and the massive (Reggeized) gluons that are also in the theory. For SU(2) color zero we can distinguish two classes of multigluon states, as follows. First we introduce the color charge conjugation operator for both gluons and quarks. For a gluon field, with color matrix $A_{\alpha\beta}^i$, color charge conjugation C gives

$$A_{\alpha\beta}^i \rightarrow -A_{\beta\alpha}^i \quad (3.15)$$

while a quark with a given helicity is transformed to an antiquark of the opposite helicity. We can also define the signature τ of a multigluon state as $\tau = \pm 1$ for an even or odd numbers of gluons. There are, essentially, two distinct color zero combinations of gluon fields, i.e.

$$\text{Tr}\{\delta_{ij} A^i A^j\}, \quad \text{Tr}\{\epsilon_{ijk} A^i A^j A^k\} \quad (3.16)$$

which both have $C = +1$ but can, respectively, create $\tau = +1$ and $\tau = -1$ states. However, since a multigluon state inherits the signature of a multi-Reggeon state, τ must satisfy

$$\tau = CP \quad (3.17)$$

where P and C are, respectively, the behavior of the coupling of the multigluon state under the parity and color charge conjugation operations. In perturbation theory such couplings have $P = +1$ for color zero. $P = -1$ corresponds to ‘‘abnormal’’ parity (as would be required for the coupling of a color zero axial vector—such as the winding-number current). From Eqs. (3.16) and (3.17), it then follows that only even signature combinations of gluons can couple. Odd signature multigluon states can couple only via the abnormal parity properties of the anomaly couplings that we discuss

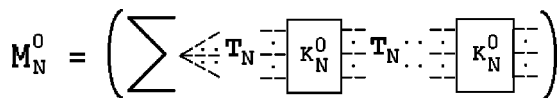


FIG. 7. Diagrams contributing to M_N^0 .

next. However, a kernel describing the interaction of massless and massive gluons will not contain any anomaly and so, as illustrated in Fig. 8, it will vanish for odd-signature combinations of massless gluons. In the following we will also need to assume that, at least for λ_\perp sufficiently small, when odd signature gluons do couple (via an anomaly coupling) and then interact amongst themselves the $M_N^0(J, \dots)$ given by Fig. 7 is not singular for $J \geq 1$. This will justify our extraction of an overall scaling divergence from what, in lowest order, is just a simple, odd-signature, multigluon state.

We will need only elementary properties of quark (and antiquark) transverse momentum diagrams. Although we will not need to discuss Reggeization effects in any detail, it is important that massless gluons again produce infrared divergences in multiquark transverse momentum kernels defined analogously to the multigluon kernels. Again, also, the exponentiation of Reggeization implies that only color zero states survive. In fact, because our introduction of Regge kinematics will be to some extent artificial, even the use of transverse momentum diagrams for quarks will seem, in part, to be forced. If the ‘‘full multi-Regge’’ calculation, to which we refer at various points in this paper, were to be carried out then quark transverse momentum diagrams would appear directly and naturally. Color zero quark (and antiquark) states would be directly selected by infrared divergences.

For fermions, in addition to using light-cone momenta $k_\pm = (k_0 \pm k_1)/\sqrt{2}$, it is convenient [28] to use complex momenta $\kappa = k_2 + ik_3$ to describe transverse momenta and also to use a corresponding notation for transverse γ matrices, i.e.

$$\gamma = (\gamma_2 + i\gamma_3)/\sqrt{2}, \quad (3.18)$$

$$\gamma^* = (\gamma_2 - i\gamma_3)/\sqrt{2}.$$

We then have

$$\gamma^2 = \gamma^{*2} = 0, \quad \gamma\gamma^* + \gamma^*\gamma = 2. \quad (3.19)$$

In the Regge limit the transverse part of an exchanged fermion propagator dominates, i.e. for a massless fermion

$$\frac{\not{k}}{k^2} \rightarrow \frac{1}{2} \left(\gamma^* \frac{1}{\kappa^*} + \gamma \frac{1}{\kappa} \right) \quad (3.20)$$

where the two terms represent the two different chiralities. For two fermion exchange the combination of opposite sign chiralities dominates and so the transverse momentum state corresponding to Eq. (3.9) is

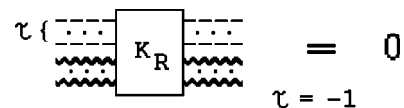


FIG. 8. Interaction of massive and massless gluons.

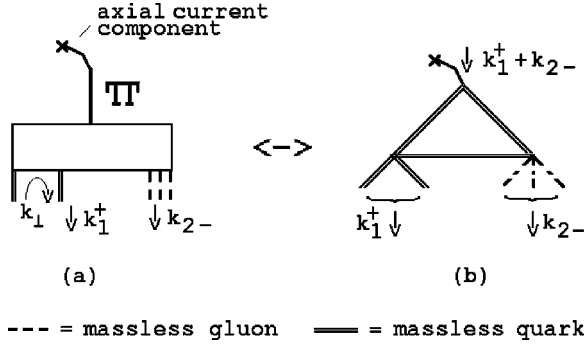


FIG. 9. (a) Pion components; (b) the anomaly coupling.

$$F_2 = \frac{1}{J} \int d^2\kappa_1 d^2\kappa_2 \left(\frac{\gamma}{\kappa_1} \otimes \frac{\gamma}{\kappa_2} + \frac{\gamma^*}{\kappa_1^*} \otimes \frac{\gamma^*}{\kappa_2^*} \right) \quad (3.21)$$

where the \otimes sign indicates that the two γ matrices are separately associated with the two fermion lines.

C. Pion couplings to wee gluons

We now generalize the light-cone analysis of the triangle anomaly pole in the previous section to derive further anomaly pole couplings involving wee gluons. It will be helpful to describe these couplings before we discuss their role in producing high-energy scattering amplitudes.

The massless pion (and nucleon) Goldstone states we create will have two distinct components, as illustrated in Fig. 9(a). A massless pion, with light-cone momentum k_1^+ , will contain an (odd-signature, color zero) “wee-gluon” component with light-cone momentum k_2^- (where $k_2^-/k_1^+ \rightarrow 0$) together with a massless quark-antiquark pair that carries the flavor quantum numbers and the light-cone momentum k_1^+ . The pion coupling to both components will be provided by the triangle diagram anomaly as illustrated in Fig. 9(b). We discuss a diagram containing three massless gluons since this is the simplest color zero, odd signature, multigluon state of the kind discussed in the previous subsection. Our discussion will easily generalize to any number of massless gluons coupling at adjacent points. The anomaly couplings we obtain will imply that the leading high-energy behavior in pion scattering arises when either the quark or the antiquark carries all the light-cone momentum k_1^+ . For our immediate discussion we will take it to be the quark that carries this momentum.

Figure 9(b) contains two “effective vertices” that are each obtained by placing propagators on shell in a larger diagram, as illustrated in Fig. 10. As in our discussion of the elementary triangle diagram we justify keeping only the anomaly pole part of the diagram by appropriately restricting the internal momentum region. As we discuss in the following subsection, the on-shell propagators will then arise consistently from longitudinal momentum integrations (that are external to the triangle). We again allow lightlike momenta k_1^+ and k_2^- to flow through the diagram and generate the numerator factors shown. The pion mass shell will be approached in the limit that we take $k_2^- \rightarrow 0$ with k_1^+ kept fixed. In this limit, therefore, the massless gluons become wee gluons.

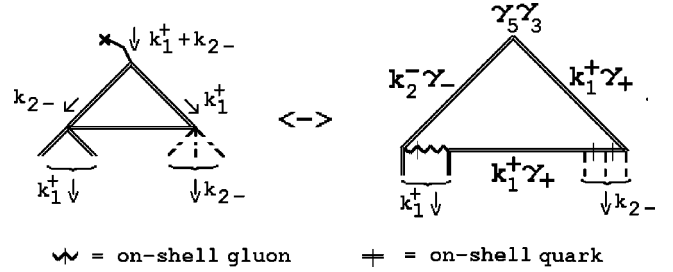


FIG. 10. Reduction to a triangle.

The generation of an effective vertex for the wee gluons is straightforward and is illustrated in Fig. 11. The wee gluons will all carry the same (longitudinal) polarization and so, as the hatched lines in Fig. 11 are placed on-shell, we will obtain an effective vertex

$$\begin{aligned} & \gamma_- \int \frac{dk'_1 + \gamma_+ k_1^+}{k'_1 + k_1^+ + \dots} \gamma_- \int \frac{dk'_2 + \gamma_+ k_1^+}{k'_2 + k_1^+ + \dots} \gamma_- \\ & = \gamma_- \gamma_+ \gamma_- \gamma_+ \gamma_- = 4 \gamma_- . \end{aligned} \quad (3.22)$$

We will give more details on how these integrations arise later.

The generation of an effective vertex involving the external quark-antiquark pair is a little more complicated. Because the internal quark and antiquark carry distinct quantum numbers they can interact only by gluon exchange. To obtain a gauge-invariant transverse momentum diagram the gluon must be on-shell. In a conventional transverse momentum diagram the produced quark-antiquark pair would have opposite chiralities [to couple to the transverse momentum state (3.21)]. This will not be the case in our analysis since the quark-antiquark pair will carry the light-cone momentum k_1^+ . However, as we discuss further in the following, we expect our analysis to be the continuation to lightlike pion momentum of spacelike Reggeized pion exchange within which the quark-antiquark pair would appear as a transverse momentum state.

The interaction needed to produce a quark-antiquark pair (with opposite chiralities) in a transverse momentum state has the γ -matrix structure shown in Fig. 12(a). The quark-antiquark interaction that we will need is shown in Fig. 12(b). In both cases we have included the (upper) γ matrices that come from the internal numerators of the triangle diagram as well as the (lower) γ matrices associated with the propagating quark-antiquark state. The middle γ matrices are the couplings to be produced by the exchanged gluon. In the “needed interaction,” one γ_\perp interaction will be necessary to obtain the anomaly numerator. In our case we will need γ_2 because we will specifically choose the $\{3\}$ component of the axial vector current generating the triangle diagrams we

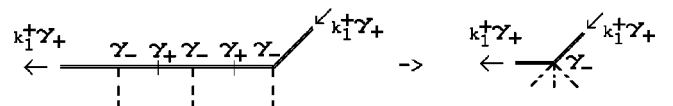


FIG. 11. Generation of an effective vertex.

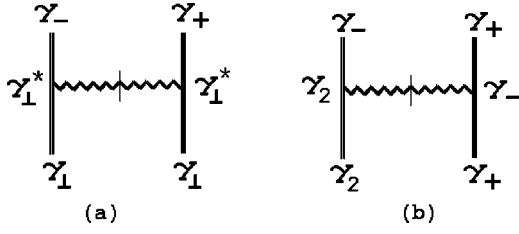


FIG. 12. (a) Production of a transverse state; (b) the needed interaction.

utilize (see Fig. 15 below). The replacement of the second γ_{\perp} interaction by γ_{-} is necessary to allow the quark to carry a lightlike momentum implying, of course, that the spin structure of the quark-antiquark state cannot be symmetric.

The γ -matrix structure of the interaction due to the exchange of an on-shell massless gluon can be written as

$$\sum_{i=1}^4 \gamma^i \otimes \gamma_i = \gamma^+ \otimes \gamma_+ + \gamma^- \otimes \gamma_- + \gamma_{\perp}^* \otimes \gamma_{\perp} + \gamma_{\perp} \otimes \gamma_{\perp}^* \quad (3.23)$$

where the \otimes factor indicates that the two γ matrices operate on distinct fermion lines. The diagonal nature of this interaction implies that it cannot produce either the interaction of Fig. 12(a) or that of Fig. 12(b). The exchange of an on-shell massive gluon with mass M_C produces, however, an additional interaction

$$\frac{\gamma \cdot \hat{k} \otimes \gamma \cdot \hat{k}}{M_C^2} \quad (3.24)$$

where \hat{k} is the momentum of the gluon. As is shown in Fig. 13, the new interaction contains the needed coupling. [It also contains the transverse state coupling of Fig. 12(a).] The γ -matrix and momentum structure of the effective vertex involving Fig. 13 is then as illustrated in Fig. 14. We have defined \tilde{k} such that k_1^+ flows directly into the quark line without flowing along the exchanged gluon line. (This will give the final high-energy behavior most directly.) In this case the \hat{k} appearing in Fig. 13 is identified with $\tilde{k} + k_2^-$ and so, as illustrated, the component of Eq. (3.24) that we need is

$$\frac{\tilde{k}_2(k_2^- + \tilde{k}^-) \gamma_2 \otimes \gamma_-}{M_C^2}. \quad (3.25)$$

In Fig. 15 we combine together the anomaly triangle diagram numerators and the γ -matrix dependence of the above effective vertices for the triangle diagram of Fig. 10. As illustrated, the resulting numerator factor is

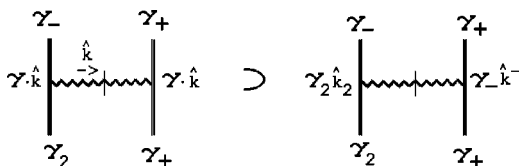


FIG. 13. The exchange of an on-shell massive vector.

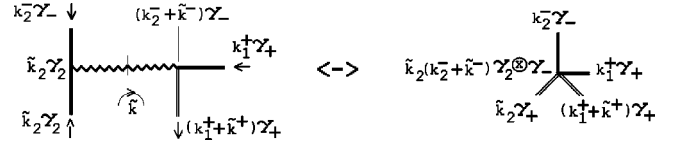


FIG. 14. Generation of a second effective vertex.

$$\begin{aligned} & \gamma_2 [k_2^- \gamma_-] \gamma_5 \gamma_3 [k_1^+ \gamma_+] \gamma_- [k_1^+ \gamma_+] \gamma_- \\ &= -2 \gamma_5 \gamma_2 \gamma_- \gamma_3 \gamma_+ \gamma_- (k_1^+)^2 k_2^- \\ &= -4 \gamma_- \gamma_5^2 (k_1^+)^2 k_2^- + \dots \\ &= -4 \gamma_- (k_1^+)^2 k_2^- + \dots \end{aligned} \quad (3.26)$$

which includes the anomaly numerator, together with an additional γ_- that couples to the produced quark-antiquark pair. The role of the γ_2 coupling in producing Eq. (3.26) is clear.

We will put the exchanged gluon on mass shell via the \tilde{k}^+ integration. Including the numerator factor of $(\tilde{k}^- + k_2^-)$ that appears in Eq. (3.25) this integration has the form

$$\int \frac{d\tilde{k}^+ (\tilde{k}^- + k_2^-) \gamma_-}{2(\tilde{k}^- + k_2^-) \tilde{k}^+ - \tilde{k}_1^2 - M_C^2} \times \dots \sim \gamma_- \quad (3.27)$$

The momentum dependence of the quark-antiquark effective vertex is then simply the remaining factor of \tilde{k}_2 in Eq. (3.25). The denominator of the reduced diagram coincides with that of the triangle diagram, and so the anomaly pole is generated straightforwardly. The full anomaly pole amplitude produced by Fig. 9(a) is therefore

$$\gamma_- \frac{[(k_1^+)^2 k_2^- \tilde{k}_2]}{M_C^2 q^2}. \quad (3.28)$$

The presence of a massive gluon is clearly crucial for the generation of this amplitude. [Since we are not going to sum diagrams nor include color factors in our discussion we will also (effectively) ignore all numerical factors.]

D. The four-current amplitude and the contributing diagrams

A major purpose of the approach developed in this paper is to avoid, as much as possible, the multi-Regge theory that has been a feature of our previous papers. Our intention is to focus directly on properties of the anomaly and thus to arrive, as directly as is possible, at the dynamical interactions of pions (and nucleons). Having the above pion couplings in

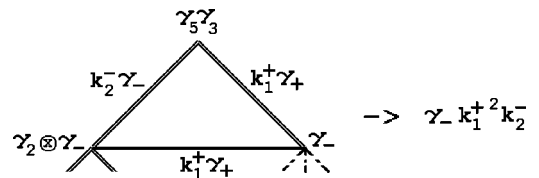


FIG. 15. The full anomaly numerator.

hand, it might be anticipated that we could obtain a pion scattering amplitude by considering a four axial vector current amplitude

$$M_{\mu_1\mu_2\mu_3\mu}(p_1,p_2,p_3,p_4) = \langle A_{\mu_1}^1(p_1)A_{\mu_2}^2(p_2)A_{\mu_3}^3(p_3)A_{\mu_4}^4(p_4) \rangle \quad (3.29)$$

in which the currents carry flavor quantum numbers such that pion (or nucleon) scattering could appear. If there is confinement [of SU(2) color] and chiral symmetry breaking, we expect to find a contribution to the current amplitude of the form (with a momentum conserving δ function removed)

$$M_{\mu_1\mu_2\mu_3\mu} \xrightarrow{p_1^2,p_2^2,p_3^2,p_4^2 \rightarrow 0} \frac{P_{1\mu_1}P_{2\mu_2}P_{3\mu_3}P_{4\mu_4}}{P_1^2P_2^2P_3^2P_4^2} \times A(s,t) + \dots \quad (3.30)$$

where $s=(p_1+p_3)^2$, $t=(p_1+p_2)^2$ and, up to a normalization factor, $A(s,t)$ is the pion scattering amplitude. The omitted terms are less singular as $p_i^2 \rightarrow 0, i=1, \dots, 4$.

We would not expect, of course, to be able to find the pion amplitude $A(s,t)$ at finite momentum. Instead, we might anticipate that combining the Regge limit ($s \rightarrow \infty$, t fixed) with the mass-shell limit ($p_i^2 \rightarrow 0, i=1, \dots, 4$) would enable us to exploit the infinite momentum properties of the anomaly discussed in the previous section. We would look for the appearance of pion poles via the anomaly pole interactions discussed above. Isolating the anomaly pole dynamically (i.e. within a larger diagram) is, however, highly nontrivial. To proceed without multi-Regge theory we will have to follow a procedure which may appear contrived, if not artificial. It will, nevertheless, have the significant advantage of taking us directly to the high-energy pion scattering amplitude. While we will briefly explain how the procedure would be fully justified within a complete multi-Regge analysis, we will be able to stay away from the full calculation. We will indeed consider a four-current amplitude but the currents will not be simple local operators. We will also describe the formation of amplitudes in terms of diagrams that can be thought of, initially, as Feynman diagrams. However, many of the integration regions in the diagrams will be cutoff, or even removed altogether. Before amplifying on our procedure, or discussing the justification, we first describe the kinds of diagrams that will be involved.

To have all the necessary anomaly effects present the diagrams must, unfortunately perhaps, be extremely complicated. Even though almost all of this complexity will gradually drop away as we proceed towards a physical pion scattering amplitude. The simplest class of diagrams which combine all the anomaly interactions are those shown in Fig. 16(a). As indicated, the diagrams contain both massless and massive gluons together with massless quarks. From diagrams of the form shown in Fig. 16(a), we will obtain pion scattering via Pomeron exchange as illustrated in Fig. 16(b). The F_i amplitudes contain diagrams that will generate the flavor anomaly and a pion pole as described above. The U

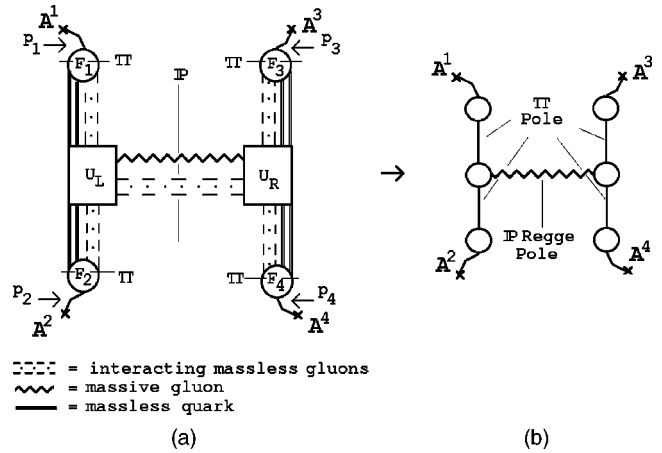


FIG. 16. (a) The simplest diagrams; (b) $\pi-\pi$ scattering via Pomeron exchange.

amplitudes contain diagrams that will generate the U(1) anomaly, as described in [13] and [14]. The U amplitudes will provide the coupling of the pion to the ‘‘Pomeron’’ that is exchanged in the Regge limit.

Having discussed the diagrams that generate the flavor anomaly in the previous subsection it will be helpful, at this point, to give the structure of the diagrams contributing to U_L . Apart from the substitution of a quark-antiquark pair for a gluon, these are essentially the diagrams discussed in [13]. The simplest diagrams have the form shown in Fig. 17. As illustrated schematically in Fig. 18, if the hatched lines are placed on-shell the diagram of Fig. 17 reduces to a triangle diagram containing the anomaly. A crucial feature of this reduction is that the ‘‘anomaly pole’’ is integrated over and so, as illustrated, is manifest as a δ function that factorizes the transverse momentum dependence of the wee gluon interaction and the ‘‘parton interaction’’ of the quarks and massive gluons. To give more details of this reduction we will need the kinematics used to discuss the full diagrams of Fig. 16(a).

Let us first assume that (schematically) the diagrams of Fig. 16(a) are generated by full Feynman diagrams involving local axial vector currents. In the next subsection we will expose the subtleties which imply that this cannot be the case. This will lead directly to an amended procedure, which we then follow. We would like each F_i amplitude to be an anomaly pole amplitude derived, in principle, from underlying diagrams within which, a loop integration is restricted to the region (2.41). In this region a light-cone momentum circulates which is essentially the corresponding external (pion) momentum. This momentum is ‘‘large’’ compared to the zero mass of the gluons. The central idea would be that, in the combined Regge and mass-shell limit, the dominant contribution to the full amplitude is obtained from this region of integration. We would argue that the internal large light-cone momenta will combine with the external Regge limit to produce similar results to a multi-Regge limit in that we will be allowed to treat all the massless gluons as if they were exchanged in a Regge kinematic regime. As a result many propagators will be placed on shell, including those that reduce the F amplitude to an effective triangle diagram that

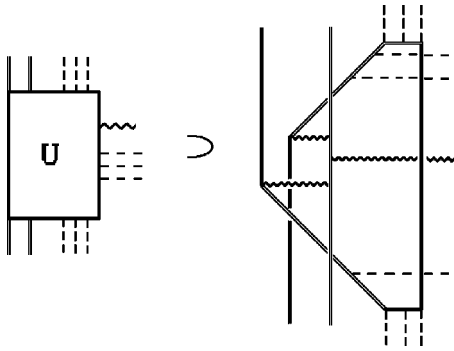


FIG. 17. One of the simplest diagrams contributing to U_L .

contains the flavor anomaly as described in the previous subsection. Similarly, within the U -amplitude lines will be placed on shell by both the external Regge limit and the internal “Regge limit” of the massless gluons such that the triangle diagrams appear that contain the $(U(1))$ anomaly. As with the flavor anomaly, the internal integration can be restricted to a light-cone region such that the anomaly interaction is separated out.

Provided the massless gluon configurations reduce to transverse momentum diagrams as we have just described we would expect, *a priori*, that the violation of gauge invariance associated with isolating the anomaly pole will produce the logarithmic scaling divergence discussed in Sec. III B. We would expect this divergence to occur separately for all odd-signature massless gluon combinations, since interactions which iterate this divergence are absent in this case. Therefore, in the “dominant” (divergent) contribution from diagrams of the form of Fig. 16(a), all the massless gluons should carry zero transverse momentum. This, in turn, would appear to self-consistently justify keeping only the anomaly pole part of the F and U amplitudes.

E. Dynamical isolation of the anomaly pole

As we saw in Sec. II, the lightlike kinematic configurations in which the anomaly pole appears in the triangle diagram are extremely special. Consequently, as we noted

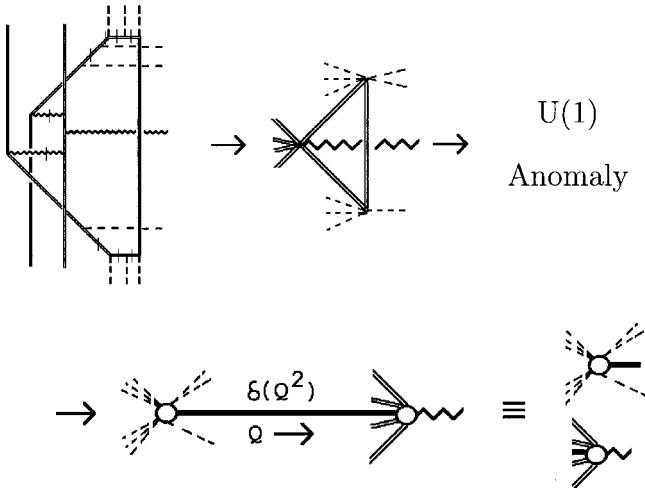


FIG. 18. Producing the $U(1)$ anomaly.

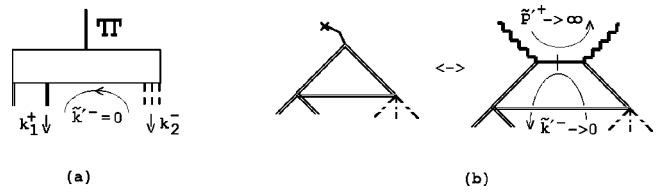


FIG. 19. (a) $\tilde{k}'^-=0$; (b) the $\tilde{P}'^+\rightarrow\infty$ coupling.

above, isolating its occurrence within larger diagrams is very nontrivial. In particular, if we use the full uncut diagram of Fig. 10 as an axial current coupling, except that the internal loop integration is restricted to the region (2.41), then we have the following problem with the above schematic procedure. When the uncut diagram appears as part of a much bigger diagram, as it should do in the diagrams of Fig. 16(a), the integration restriction is not actually sufficient to induce the Regge kinematics we want. Even if it were, the light-like momentum configurations produced by multigluon transverse momentum divergences, although very close to those in which the anomaly pole appears, would not be quite what is needed.

These problems are caused because when the diagram that gives the pion coupling of Fig. 9(a) is a component of a larger diagram, the light-cone momentum denoted by \tilde{k}'^- in Fig. 19(a) should be integrated over. The presence of this momentum has two effects. First it gives a mass $\sim\tilde{k}'^-k_1^+$ to the quark-antiquark pair that prevents the appearance of the pion anomaly pole. Secondly, if it flows through any of the massless gluon propagators, it will combine with the lightlike momentum flowing in from the U amplitude to remove the transverse momentum divergence of the massless gluon state.

To remove these problems we make the momentum restriction that $\tilde{k}'^-=0$, i.e. \tilde{k}'^- is not integrated over. This will allow us to follow explicitly the schematic procedure outlined in the previous subsection. In effect, though, it is this restriction that generates the logarithmic transverse momentum divergences which are the cornerstone of our dynamics. Within this presentation, it may therefore appear artificial and perhaps even unphysical at first sight. However, this restriction would automatically appear if the current was not a simple local operator but was instead a nonlocal current component that originates from a further external infinite momentum limit as illustrated in Fig. 19(b). (As would be exactly the case if we used multi-Regge theory to first obtain the pion as a spacelike Reggeized state.) In this case, the axial vector current component is an effective point coupling derived by placing an intermediate quark state on shell, via an integration over \tilde{k}'^- . (Using the \tilde{k}'^- integration for this purpose leaves intact the full loop integration generating the anomaly.)

Probably, the feature that local axial vector currents are not only not needed but are not wanted in our formalism is a deep matter of principle. It seems to be essential that our pion be extracted as a wee-parton component of additional infinite momentum external states. (Effectively exploiting the “triviality of the infinite momentum vacuum” to the

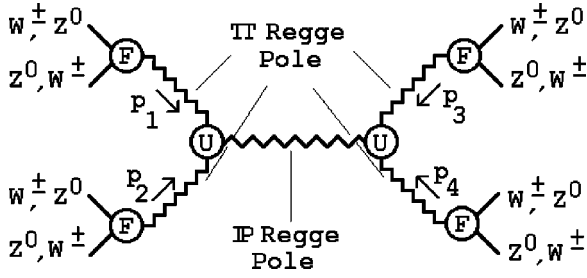


FIG. 20. A multi-Regge amplitude.

maximum.) The additional external states should be vector particles with the appropriate polarizations to induce an axial vector current vertex. It is interesting (and perhaps also a deep feature of our procedure) that the quantum numbers involved imply these particles could actually be W s and Z^0 .

Although it would be a more complicated calculation, there would be other advantages in making the further infinite momentum limit part of our discussion. In particular it would eliminate the need to appeal to the phase-space restriction involved in generating the anomaly pole to justify placing the hatched lines of the anomaly generating diagrams on shell. Indeed, it should now be clear that if we want to proceed systematically we cannot really avoid multi-Regge theory and we are paying a heavy price by trying to do so. If we simply studied the limit producing the multi-Regge amplitude of Fig. 20 no questionable procedures would be necessary. The appearance of the reduced triangle diagram in the coupling of the external W and Z_0 states would be (complicated but) straightforward in principle. The anomaly (or pion) pole would directly appear in conjunction with the transverse momentum divergences. The one subtlety that would remain would be the interplay between the ultraviolet and infrared contributions of both the chiral and $U(1)$ anomalies. However, we will not elaborate on this here.

It is important to note that, in this paper, we will isolate the anomaly pole (in principle by a phase-space restriction) in all the anomaly subdiagrams within our amplitudes. In [15] we proposed starting with initial states that had effectively the same wee gluon content as the pions we create via the anomaly pole. However, we then allowed them to scatter into arbitrary multi-Reggeon states and argued that the anomaly interactions generate an overall logarithmic infrared divergence that selects the allowed physical states and amplitudes. In the present discussion, we will require pion poles in both the initial and final states. Nevertheless, for subtle reasons the overall divergence will remain logarithmic.

As a final point, before we proceed to the construction of actual amplitudes, we note that that we will impose a cutoff in all transverse momenta. This has a dual purpose. First, to obtain contributions from “relatively simple” (gauge-dependent) Feynman diagrams to gauge-invariant transverse momentum diagrams (that have contributions, of course, from many Feynman diagrams). Secondly we will want to exploit the infrared scaling properties of multigluon transverse momentum diagrams that lead to infrared divergences as discussed in the above subsection. Our final results will be

presented entirely in terms of transverse momentum diagrams or, at a later stage, Reggeon diagrams.

F. Light-cone momenta and Lorentz frames

Light-cone momenta are clearly a central feature of our discussion. In discussing the various components of diagrams of the form of Fig. 16(a) we will need to allow for a variety of light-cone momenta, both externally and as integration variables. In particular, to introduce the triple-Regge $U(1)$ anomaly interaction the wee gluons in an outgoing pion must be associated with a light cone whose space direction is orthogonal to that of the incoming wee gluon light cone. To describe this we will need to introduce some new light-cone notation. In addition we will need to introduce a set of Lorentz frames in which the various external momenta take specific forms.

We begin in what we will call the “finite momentum frame” \mathcal{F}_L for the left-hand part of Fig. 16(a). In this frame we write

$$\begin{aligned} p_1 &= k^{1+} + q^{1-} \\ &= k_{1-} + q_{1+} \\ &= \left(\frac{k}{\sqrt{2}}, \frac{k}{\sqrt{2}}, 0, 0 \right) + \left(\frac{q}{\sqrt{2}}, -\frac{q}{\sqrt{2}}, 0, 0 \right). \end{aligned} \quad (3.31)$$

The notation is straightforward in that k^{1+} is a vector with raised index component along the light cone defined by the positive $\{1\}$ axis (and all other orthogonal components are zero). Similarly q^{1-} is a vector with raised index component along the light cone defined by the negative $\{1\}$ axis. The same vectors can be labeled via lowered index components as usual. We similarly write

$$\begin{aligned} p_2 &= -k^{2+} - q^{2-} \\ &= -k_{2-} - q_{2+} \\ &= -\left(\frac{k}{\sqrt{2}}, 0, \frac{k}{\sqrt{2}}, 0 \right) - \left(\frac{q}{\sqrt{2}}, 0, -\frac{q}{\sqrt{2}}, 0 \right) \end{aligned} \quad (3.32)$$

where now k^{2+} is a vector with raised index component along the light cone defined by the positive $\{2\}$ axis while q^{2-} is a vector with raised index component along the light cone defined by the negative $\{2\}$ axis. Since

$$p_1^2 = p_2^2 = 2kq \quad (3.33)$$

we see that

$$q \rightarrow 0 \Rightarrow p_1^2, p_2^2 \rightarrow 0. \quad (3.34)$$

In the “infinite momentum frame” \mathcal{F}_I , in which we will consider the complete scattering process, the momenta p_1 and p_2 are obtained from their finite momentum frame forms by applying a boost $a_z(\zeta)$ along the z axis. If $C = \cosh \zeta$ and $S = \sinh \zeta$ then

$$p_1 = \left(C \frac{k+q}{\sqrt{2}}, \frac{k-q}{\sqrt{2}}, 0, S \frac{k+q}{\sqrt{2}} \right) \quad (3.35)$$

and

$$p_2 = - \left(C \frac{k+q}{\sqrt{2}}, 0, \frac{k-q}{\sqrt{2}}, S \frac{k+q}{\sqrt{2}} \right). \quad (3.36)$$

Similarly, in the ‘‘finite momentum frame’’ \mathcal{F}_R the momenta entering the right-hand part of Fig. 16(a) have the form

$$\begin{aligned} p_3 &= k^{2+} + q^{2-} \\ &= \left(\frac{k}{\sqrt{2}}, 0, \frac{k}{\sqrt{2}}, 0 \right) + \left(\frac{q}{\sqrt{2}}, 0, \frac{-q}{\sqrt{2}}, 0 \right) \end{aligned} \quad (3.37)$$

and

$$\begin{aligned} p_4 &= -k^{1+} - q^{1-} \\ &= - \left(\frac{k}{\sqrt{2}}, \frac{k}{\sqrt{2}}, 0, 0 \right) - \left(\frac{q}{\sqrt{2}}, -\frac{q}{\sqrt{2}}, 0, 0 \right) \end{aligned} \quad (3.38)$$

and so we also have

$$p_3^2 = p_4^2 = 2kq. \quad (3.39)$$

For the right-hand momenta, however, the infinite momentum frame \mathcal{F}_I is reached from the finite momentum frame \mathcal{F}_R by applying a boost $a_z(-\zeta)$ along the z axis. \mathcal{F}_R is therefore reached from \mathcal{F}_L by a boost $a_z(-2\zeta)$. In \mathcal{F}_I

$$p_3 = \left(C \frac{k+q}{\sqrt{2}}, 0, \frac{k-q}{\sqrt{2}}, -S \frac{k+q}{\sqrt{2}} \right) \quad (3.40)$$

and

$$p_4 = - \left(C \frac{k+q}{\sqrt{2}}, \frac{k-q}{\sqrt{2}}, 0, -S \frac{k+q}{\sqrt{2}} \right). \quad (3.41)$$

Evaluating all momenta in \mathcal{F}_I we have

$$s = (p_1 + p_3)^2 = (p_2 + p_4)^2 \xrightarrow{q \rightarrow 0} (C^2 + S^2)k^2 \sim_{C \rightarrow \infty} 2C^2k^2 \quad (3.42)$$

$$t = (p_1 + p_2)^2 \xrightarrow{q \rightarrow 0} -k^2. \quad (3.43)$$

Therefore, we now have three external momentum scales, in addition to one mass scale, in our discussion, i.e.

$$q^2 \ll M_C^2 \ll k^2 \ll s. \quad (3.44)$$

The mass-shell limit is now $q \rightarrow 0$ and the Regge limit $s/t \rightarrow \infty$ is obtained as $C \rightarrow \infty$. In the following we will combine these limits by taking

$$q \sim 1/C \rightarrow 0, \quad qC \gg M_C. \quad (3.45)$$

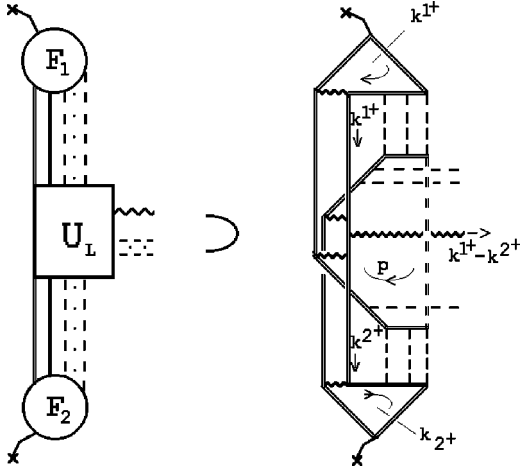
G. Constructing amplitudes

To construct amplitudes corresponding to the diagrams of Fig. 16(a) we proceed as outlined in the above subsections. We first consider Fig. 9 as a one loop Feynman diagram within F_1 and ignore the hatches. We consider the analogous diagram within F_2 and connect the two diagrams with the U_L diagram of Fig. 17 to obtain the full diagram shown in Fig. 21. (The double-dashed line carries zero momentum within the anomaly configuration that will be discussed later.) If we then treat this diagram as a subdiagram and join it with its own reflection we obtain a complete diagram of the form shown in Fig. 16(a). The left and right-hand subdiagrams will be joined only by the exchanged gluons (three massless and one massive), which will carry finite transverse momentum (in all three Lorentz frames). The relevant parts of the left and right-hand subdiagrams will have analogous forms in the \mathcal{F}_L and \mathcal{F}_R frames, respectively, and will be in a relative Regge limit in the \mathcal{F}_I frame. The combination of the Regge limit with the phase space restrictions we impose will, as anticipated, place a large number of lines on-shell such that the central quark loop within U_L reduces to a triangle diagram as illustrated schematically in Fig. 18. The crucial element will be, of course, that this diagram also contains the anomaly pole. To understand this we must determine all the effective vertices that are produced by the reduction to transverse momentum integrals.

To discuss the diagram of Fig. 21, we will begin in the \mathcal{F}_L frame and as we evaluate each part of the diagram we will discuss the effect of transforming to the \mathcal{F}_I frame. In the \mathcal{F}_L frame p_1 and p_2 are given, respectively, by Eqs. (3.31) and (3.32). We direct the large light-cone momenta k^{1+} and k^{2+} through the diagram as shown and restrict the integration in both F_i diagrams to the momentum region corresponding to Eq. (2.41). Note that

$$\begin{aligned} k^{1+} - k^{2+} &= \left(\frac{k}{\sqrt{2}}, \frac{k}{\sqrt{2}}, 0, 0 \right) - \left(\frac{k}{\sqrt{2}}, 0, \frac{k}{\sqrt{2}}, 0 \right) \\ &= \left(0, \frac{k}{\sqrt{2}}, -\frac{k}{\sqrt{2}}, 0 \right) \end{aligned} \quad (3.46)$$

is a spacelike momentum lying in the $\{x, y\}$ plane. We introduce notation for all the loop momenta of Fig. 21 in Fig. 22. We show only that part of the diagram involving F_1 and part of U_L . The part containing F_2 can obviously be discussed analogously. The hatched lines are those placed on shell by longitudinal momentum integrations and each of the hatches is labeled by the index for the momentum involved. We discuss each integration separately as follows.


 FIG. 21. Connecting the F_1 and F_2 amplitudes.

H. The massless gluons

Provided the loop momentum p in the lower part of Fig. 22 is much less than k_1^+ (as will be the case in the anomaly pole contribution we will extract) the k'_i integrations over the momenta of the vertical massless gluon exchanges can be reduced to transverse momentum diagrams by placing the

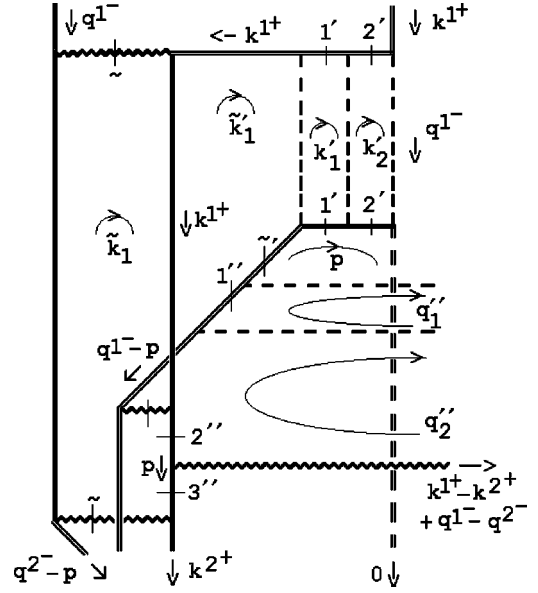


FIG. 22. Notation for Fig. 21.

hatched fermion lines on shell. We can illustrate this (very well-known) procedure as follows. Using conventional light-cone coordinates, which in the notation of Sec. III F correspond to light-cone vectors k'^{1+} and k'^{1-} , we can write

$$\begin{aligned}
 & \int d^4 k'_1 d^4 k'_2 \left\{ \frac{\gamma^\mu \gamma \cdot (k'_1 - k^{1+} + q^{1-}) \gamma^\nu \gamma \cdot (k'_2 - k^{1+} + q^{1-}) \gamma^\tau}{(k'_1 - k^{1+} + q^{1-})^2 (k'_2 - k^{1+} + q^{1-})^2} \right\} \\
 & \otimes \left\{ \frac{\gamma_\mu \gamma \cdot (p - k'_1 - q^{1-}) \gamma_\nu \gamma \cdot (p - k'_2 - q^{1-}) \gamma_\tau}{(p - k'_1 - q^{1-})^2 (p - k'_2 - q^{1-})^2} \right\} \frac{1}{(k'_1 - \bar{k}'_1)^2 (k'_2 - k'_1)^2 (k'_2 + q^{1-})^2} \\
 & \sim \left\{ \gamma^\mu \frac{\int dk'_1{}^- \gamma_+ k^{1+}}{(k'_1{}^- - k^{1+} + \dots)^2} \gamma^\nu \frac{\int dk'_2{}^- \gamma_+ k^{1+}}{(k'_2{}^- - k^{1+} + \dots)^2} \gamma^\tau \right\} \otimes \left\{ \gamma_\mu \frac{\int dk'_1{}^+ \gamma_+ p^+}{(k'_1{}^+ + p^+ + \dots)^2} \gamma_\nu \frac{\int dk'_2{}^+ \gamma_+ p^+}{(k'_2{}^+ + p^+ + \dots)^2} \gamma_\tau \right\} \\
 & \times \int d^2 k'_{1\perp} d^2 k'_{2\perp} \frac{1}{(k'_{1\perp} - \bar{k}'_{1\perp})^2 (k'_{2\perp} - k'_{1\perp})^2 (k'_{2\perp})^2} \\
 & \sim \gamma^+ \otimes \gamma_+ \int d^2 k'_{1\perp} d^2 k'_{2\perp} d^2 k'_{3\perp} \frac{\delta^2 \left(\bar{k}'_{1\perp} - \sum_i k_{i\perp} \right)}{(k'_{1\perp} - \bar{k}'_{1\perp})^2 (k'_{2\perp} - k'_{1\perp})^2 (k'_{2\perp})^2} \quad (3.47)
 \end{aligned}$$

which is a transverse state of the kind discussed in Sec. III B. This illustrates how the integrals (3.22) arise. Also the γ^+ ($= \gamma_-$) factor is the effective vertex appearing in Fig. 11.

Equation (3.47) is, as anticipated, infrared divergent. As we discussed at length in Sec. III B, if the three gluon state carries color all of the divergences will exponentiate in higher orders. If it carries color zero the only divergence which will not exponentiate is the overall divergence that

potentially occurs when $\bar{k}'_{1\perp}$ is integrated over and the $k'_{i\perp}$ are scaled uniformly to zero. If this divergence is present and we isolate its contribution, the massless multigluon propagators will contribute only at zero momentum and there will be no effect in transforming their contribution from the \mathcal{F}_L frame to the \mathcal{F}_I frame. (While the contribution of the anomaly amplitudes to which the multigluon states couple will depend on the small light-cone momentum q^{1-} , the con-

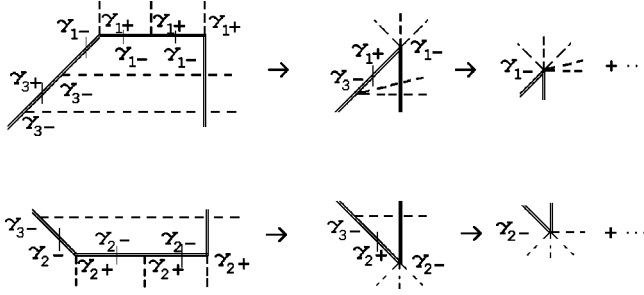


FIG. 23. Massless gluon effective vertices.

tribution of the transverse propagators and interactions will be independent of this momentum.) To discuss the exact nature of the divergence we must include the effective vertices provided by the anomaly amplitudes and the contribution of the quark-antiquark state.

For the reasons discussed in Sec. III E, we do not integrate over \tilde{k}'_1^- and so at $\tilde{k}'_{1\perp}=0$ the effective vertex provided by the F_1 amplitude will be the anomaly pole amplitude of Eq. (3.28). In frame \mathcal{F}_I we will use Eq. (2.55) which gives the pion coupling after the current momentum factor has been removed. In the present notation the full effective vertex provided by the F_1 amplitude is then (without the current momentum factor)

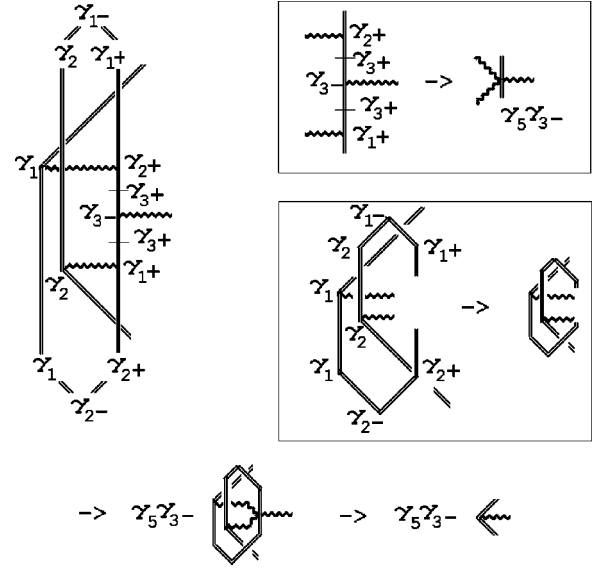
$$\tilde{k}_2 \frac{\epsilon_{\sigma\delta 3-} (k^1)^{\sigma} (q^1)^{\delta}}{q^2} \sim \tilde{k}_2 \frac{[kqC]}{M_C^2 q^2} \quad (3.48)$$

which, when qC is kept finite, gives a finite pion pole residue. Note that, since this vertex is independent of $\tilde{k}'_{1\perp}$, it will not affect the divergence at $\tilde{k}'_{1\perp}=0$. This is a crucial consequence of the absence of a vector Ward identity for the anomaly pole contribution.

In the Regge limit, the q''_1 , q''_2 and q''_3 integrations will, in analogy with Eq. (3.47), be reduced to transverse momentum integrals in the $\{x, y\}$ plane by placing on shell the labeled hatched lines. (q''_3 is the momentum of the horizontal massless gluon line attached to the bottom of the diagram.) Since the \mathcal{F}_L , \mathcal{F}_I and \mathcal{F}_R frames differ only by boosts acting in the $\{z, t\}$ plane, the q''_j transverse momentum integrations will be the same in each of the frames we discuss and will produce the same infrared divergence. If we continue to work in the \mathcal{F}_L frame the combination of the k'_i and q''_j longitudinal integrations generates the effective vertices shown in Fig. 23. We will combine these vertices to obtain the anomaly amplitude produced by the U_L loop shortly.

I. Quark transverse momentum integrals

The reduction to transverse integrals of the quark loop integrations, over \tilde{k}_1 in Fig. 22 and over \tilde{k}_2 in the lower part of Fig. 21, is not straightforward. This reduction should be

FIG. 24. The γ -matrix structure generating the γ_5 vertex.

responsible for placing all of the hatched massive vector propagators on shell. However, the light-cone momenta flowing along these lines (q^{1-} and q^{2-}) is small (and zero on mass shell) in \mathcal{F}_L , although it is finite in \mathcal{F}_I . Apparently, therefore, there is no Regge limit kinematics for us to exploit. Nevertheless, we need to place the relevant lines on shell, both to obtain a gauge-invariant result in which we understand the exponentiation of infrared divergences, and to utilize the anomaly couplings.

In the full multi-Regge limit of Fig. 20 the p_i momenta would be initially taken spacelike and (as we remarked earlier) quark transverse integrals would be obtained naturally. Assuming a Reggeized pion appears, the multi-Regge amplitude will contain corresponding asymptotic dependence on invariant subenergies. This dependence should disappear as the scalar pions are placed on mass shell at $p_i^2=0$, $i=1, \dots, 4$ and the on-shell amplitude should factorize out straightforwardly. Even though the full multi-Regge amplitude is independent of the subenergies (at $p_i^2=0$) it is obtained by asymptotic expansion around infinite subenergies. Correspondingly, any transverse integrals that are involved should be initially obtained at infinite subenergies. In effect, we are attempting to obtain these integrals directly at zero subenergies by appealing only to properties of the anomaly poles generating the pions.

In fact, even with the kinematic constraints we have imposed, we will be able to place all the massive gluon lines on shell (and so, consistently, use the anomaly couplings). The result will be formally the same as carrying out the large subenergy limit but only a limited range of transverse momenta will be involved. The discontinuity that is (effectively) taken will be that of an unphysical pseudothreshold (at zero subenergy), rather than a physical normal threshold. Presumably (although we will not attempt to prove this) the unphysical chirality transition involved in the anomaly pole couplings can be viewed as producing this contribution. (In the last section we described the relationship between an un-

physical singularity and the anomaly pole and in [13] we emphasized that triple-Regge anomaly interactions are due to unphysical multiple discontinuities containing pseudothresholds.)

As we have already noted, our discussion of the effective vertex of Fig. 14 applies directly to the placing on-shell of the upper (massive gluon) line associated with the \tilde{k}_1^{1+} integration in Fig 22. The \tilde{k}_1^{1-} integration associated with the lower on-shell line is very similar and massive gluon exchange must again be involved. To see this we must establish which γ matrix couplings appear at the vertices. In fact, these couplings are almost entirely determined by the requirement that the anomaly be present in the reduced U_L diagram. The complete γ -matrix structure of Fig. 21 that is not included in Fig. 23 is shown in Fig. 24. The top and bottom trios of γ matrices in the initial figure are those due to the effective vertices of F_1 and F_2 that are analogous to Fig. 14 together with the resulting propagator components. We specifically choose the $\{3\}$ component for both the F_1 and F_2 external currents. This choice, together with the choice of the space directions for the large light-cone momenta of p_1 and p_2 , determines the relative structure of the trios. The appearance of the $\gamma_{3\pm}$ matrices is a direct consequence of the Regge limit. The upper inset in Fig. 24 shows how the identity (2.39) generates a γ_5 interaction. The participating γ_{1+} and γ_{2+} matrices have to be produced by the longitudinal momentum integrals (via massive gluon exchange), as we discuss below. The remaining γ_1 and γ_2 matrices are needed to allow the reduction of the remaining product to the unit matrix (plus terms that give zero when contracted with the massless gluon vertices), as the lower inset illustrates. It is not difficult to see that the requirement of a γ_5 interaction, together with a nonzero reduction of the remaining matrix product, determines the complete structure of Fig. 24.

In Fig. 25 we have isolated the γ -matrix structure and the relevant momenta for the quark loops that couple F_1 and F_2 in Fig. 21. Each of the γ matrices in Fig. 25 is either a vertex component of a massive gluon propagator or is a numerator component of a quark propagator. Although the γ matrices

contract, as we have already discussed, the corresponding momentum factors remain. We ignore the loop momentum p since it will be set to zero by the generation of the U(1) anomaly pole. Also, since $\tilde{k}'_{1\perp} = \tilde{k}'_{2\perp} = 0$ after the transverse momentum divergence is extracted, we first ignore both of these momenta.

The \tilde{k}_1^+ integration is given by Eq. (3.27) while the \tilde{k}_1^- integration has the form

$$\int \frac{d\tilde{k}_1^- (\tilde{k}_1^+ \gamma_+ + q^{2-} \cdot \gamma_+)}{2\tilde{k}_1^+ \tilde{k}_1^- + 2q^{2-} \cdot \tilde{k}_1 - \tilde{k}_{1\perp}^2 - M_C^2} \times \dots \sim \gamma_+ \times \dots \quad (3.49)$$

The two integrations give, respectively,

$$2\tilde{k}_1^+ \tilde{k}_1^- + 2\tilde{k}_1 \cdot q^{1-} = \tilde{k}_{1\perp}^2 + M_C^2 \quad (3.50)$$

and

$$2\tilde{k}_1^+ \tilde{k}_1^- + 2\tilde{k}_1 \cdot q^{2-} = \tilde{k}_{1\perp}^2 + M_C^2. \quad (3.51)$$

In the \mathcal{F}_I frame, q^{1-} and q^{2-} are boosted to become almost the same lightlike momentum q^{3+} , i.e.

$$\begin{aligned} q^{1-} &\sim (Cq, -q, 0, Sq) \underset{q \rightarrow 0}{\sim} q^{3+}, \\ q^{2-} &\sim (Cq, 0, -q, Sq) \underset{q \rightarrow 0}{\sim} q^{3+}, \end{aligned} \quad (3.52)$$

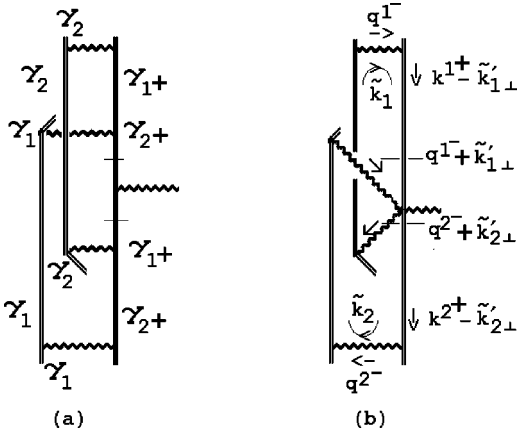
and so Eqs. (3.50) and (3.51) have a common solution as $q \rightarrow 0$ (which is why a pseudthreshold is involved) with

$$\tilde{k}_1^+ \sim \tilde{k}_1^- \sim \tilde{k}_{13} \sim \frac{M_C^2}{Cq}, \quad \tilde{k}_{12}^2 \lesssim M_C^2. \quad (3.53)$$

Incorporating all the remaining momentum factors given by the γ matrices of Fig. 25(a) (together with a factor of M_C^{-2} from the additional exchanged gluon propagator) the $\tilde{k}_{1\perp}$ transverse momentum integral has the form

$$\begin{aligned} &\frac{1}{M_C^2} \int d^2\tilde{k}_{1\perp} \{F_1 \text{ numerator}\} \times \{\text{antiquark numerator}\} \times \{\text{gluon numerator}\} \\ &\times \{\text{quark numerator}\} / \{\text{propagator denominator}\}^2 \\ &= \frac{1}{M_C^2} \int \frac{d^2\tilde{k}_{1\perp} \tilde{k}_{12} \tilde{k}_{12} (\tilde{k}_{12} + q) k^{1+}}{(\tilde{k}_1^2)^2} \end{aligned} \quad (3.54)$$

$$\sim \frac{qk^{1+}}{M_C^2} \left\{ \int_{|\tilde{k}_{13}| \sim M_C^2/Cq} d\tilde{k}_{13} \right\} \left\{ \int_{M_C^2/Cq \leq |\tilde{k}_{12}| \leq M_C} \frac{d\tilde{k}_{12}}{\tilde{k}_{12}^2} \right\} \sim \frac{qk^{1+}}{M_C^2} \left\{ \frac{M_C^2}{Cq} \right\} \left\{ \frac{Cq}{M_C^2} \right\} \sim \frac{qk^{1+}}{M_C^2} \quad (3.55)$$

FIG. 25. The quark loops: (a) γ -matrices; (b) momenta.

which gives a finite answer in the \mathcal{F}_I frame when $k^{1+} \sim C \rightarrow \infty$, with Cq kept finite. Note that the part of the integrand in Eq. (3.54) that does not vanish when $q=0$ is odd with respect to \tilde{k}_{12} and hence integrates to zero. If this were not the case, the combination of light-cone momentum factors from each fast quark numerator would give an amplitude increasing like $C^4 \sim s^2$.

Conversely, if we obtain only finite results of the form of Eq. (3.55) for each transverse momentum integral, we will not obtain any increasing behavior as $s \rightarrow \infty$. To obtain the maximally increasing amplitude, we must consider the $\tilde{k}'_{1\perp}$ dependence in more detail. If, for example, we direct \tilde{k}'_1 so that in the $\tilde{k}_{1\perp}$ integral we substitute \tilde{k}'_{12} for \tilde{k}_{12} in the anti-quark numerator in Eq. (3.55), this will give

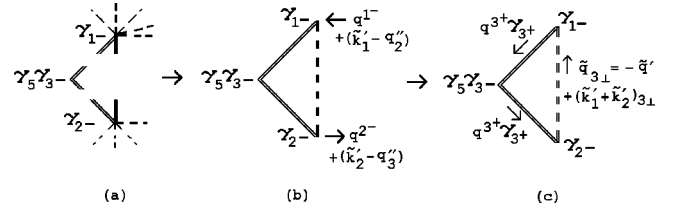
$$\frac{qk^{1+}}{M_C^2} \rightarrow \frac{\tilde{k}'_{12}k^{1+}}{M_C^2} \sim kC \xrightarrow{C \rightarrow \infty} \infty. \quad (3.56)$$

Alternatively we can keep the \tilde{k}'_{12} dependence of one of the denominators giving

$$\int \frac{d\tilde{k}_{12}\tilde{k}_{12}}{(\tilde{k}_{12}-\tilde{k}'_{12})^2\tilde{k}'_{12}} \sim \int \frac{d\tilde{k}_{12}\tilde{k}'_{12}}{\tilde{k}_{12}^2} \quad (3.57)$$

which again leads to Eq. (3.56). If we keep the contribution of the form of Eq. (3.55) from the $\tilde{k}_{2\perp}$ integral we will obtain a factor of C from the left subdiagram (of Fig. 21). Treating the transverse integrals from the right subdiagram in an analogous manner will give an amplitude increasing like $C^2 \sim s$.

Obviously we could also keep the factor of q in the $\tilde{k}_{1\perp}$ integral and keep nonleading \tilde{k}'_{21} behavior in the $\tilde{k}_{2\perp}$ integral. Either way we gain one power of the energy while reducing the degree of divergence of either the $\tilde{k}'_{1\perp}$ or the $\tilde{k}'_{2\perp}$ integration. We will see that we cannot obtain a further power of the energy by reducing the degree of divergence of all the $\tilde{k}'_{1\perp}$

FIG. 26. (a) The triangle; (b) momenta in \mathcal{F}_L ; (c) momenta in \mathcal{F}_I .

integrals since there will then be no overall transverse divergence. To see this we must consider the final part of the diagram that we have not yet discussed in detail.

J. The U(1) anomaly amplitude and the infrared divergence

As illustrated in Fig. 26(a), combining Fig. 23 and Fig. 24 produces a triangle of γ matrices which has the appropriate structure to give the anomaly. The large light-cone momenta k^{1+} and k^{2+} flow in and out of the γ_5 vertex and do not enter the triangle diagram. As shown in Fig. 26(b) the external momenta that flow through the diagram in \mathcal{F}_L are q^{1-} and q^{2-} together with the \tilde{k}'_i and the q''_i (all of which are zero in the infrared divergence configuration for the massless gluons, when the mass-shell limit is taken). In [14] we discussed, at length, momentum configurations of this kind which produce the anomaly pole. For our present purposes it is simplest to go straight to the \mathcal{F}_I frame. In this frame the timelike components of p_1 and p_2 that are $O(q)$ in the \mathcal{F}_L frame are boosted to give the finite lightlike momentum $q^{3+} \sim Cq$, as in Eq. (3.52), which then flows through the diagram as in Fig. 26(c). In this last figure we have dropped the small (transverse) momenta along lines where the finite lightlike momentum flows. If we define $\tilde{q}_{3\perp}$ to be the (small) momentum transverse to q^{3+} that is flowing through the (double) dashed vertical line then

$$\tilde{q}_{3\perp} = (\tilde{k}'_1 + \tilde{k}'_2)_{3\perp} - \tilde{q}' \quad (3.58)$$

where $\tilde{q}' = q''_2 + q''_3$. Comparison with the momentum configuration (2.42) shows that the anomaly “ δ -function amplitude” has the form

$$(q^{3+})^2 \tilde{q}_3 \delta(\tilde{q}_{3\perp}^2) \quad (3.59)$$

which sets to zero momentum the double-dashed line.

The δ function in Eq. (3.59) couples the q''_i and \tilde{k}'_j infrared divergences. As we saw above, these divergences are also modified by the need to obtain nonzero quark transverse momentum integrals. To consider the remaining divergence we keep only the scaling infrared divergence from each massless multigluon state which, as discussed in Sec. III B, is the only divergence that survives high-order exponentiation. The overall divergence that remains then has the form

$$\begin{aligned}
& \int d^2\tilde{q}'_{\perp} \{\text{multigluon scaling amplitude}\} \\
& \int d^2\tilde{k}'_{1\perp} d^2\tilde{k}'_{2\perp} \{\text{multigluon scaling amplitude}\}^2 \{\text{anomaly}\} \{\text{quark momentum}\} \\
& \int d^2\tilde{k}'_{3\perp} d^2\tilde{k}'_{4\perp} \{\text{multigluon scaling amplitude}\}^2 \{\text{anomaly}\} \{\text{quark momentum}\} \\
& \sim \int \frac{d^2\tilde{q}'_{\perp}}{\tilde{q}'_{\perp}{}^2} \int \frac{d^2\tilde{k}'_{1\perp} d^2\tilde{k}'_{2\perp}}{\tilde{k}'_{1\perp}{}^2 \tilde{k}'_{2\perp}{}^2} \delta((\tilde{q}'_{\perp} - \tilde{k}'_{1\perp} - \tilde{k}'_{2\perp})^2) (\tilde{q}'_{\perp} - \tilde{k}'_{1\perp} - \tilde{k}'_{2\perp}) \tilde{k}'_{12} \\
& \int \frac{d^2\tilde{k}'_{3\perp} d^2\tilde{k}'_{4\perp}}{\tilde{k}'_{3\perp}{}^2 \tilde{k}'_{4\perp}{}^2} \delta((\tilde{q}'_{\perp} - \tilde{k}'_{3\perp} - \tilde{k}'_{4\perp})^2) (\tilde{q}'_{\perp} - \tilde{k}'_{3\perp} - \tilde{k}'_{4\perp}) \tilde{k}'_{32} \\
& \sim \int \frac{d^2\tilde{q}'_{\perp}}{\tilde{q}'_{\perp}{}^2}
\end{aligned} \tag{3.60}$$

which is a simple logarithmic divergence as we anticipated. We will not attempt to prove that this divergence cannot be canceled by other diagrams that we have not discussed.

K. The physical scattering amplitude

We keep as the physical scattering amplitude the coefficient of the divergence (3.60)—the divergence being factorized off as a “condensate” that is to be part of the definition of a physical pion state. (We have discussed how this is consistent for Reggeon states in [14].) The physical amplitude is then given by

$$\begin{aligned}
& \prod_i \{F_i \text{ anomaly pole amplitude}\} \{\text{quark } \tilde{k}'_{i\perp} \text{ integrals}\} \prod_{j=L,R} \{U_j \text{ anomaly amplitude}\} \\
& \times \{\text{massive gluon propagator}\}
\end{aligned} \tag{3.61}$$

and so combining Eqs. (3.48), (3.55), (3.57) and (3.59) we obtain

$$\begin{aligned}
& \left(\frac{kCq}{M_C^2 q^2}\right)^4 \left(\frac{kC}{M_C^2} \frac{kCq}{M_C^2}\right)^2 (qC)^4 \frac{1}{t+M_C^2} \\
& = \left(\frac{1}{q^2}\right)^4 \left[\frac{C^2 q^2}{M_C^2}\right]^4 \left[\frac{s q^2}{M_C^4}\right] \left[\frac{t}{M_C^2}\right]^2 \left[\frac{s}{t+M_C^2}\right].
\end{aligned} \tag{3.62}$$

We have reorganized the result into the separate square brackets because each represents a different physical effect, as we now briefly discuss.

The factor of $(1/q^2)^4$ in Eq. (3.62) is, of course, the contribution of the four pion poles. All but the last two square brackets are finite constants when the limit $1/q \sim C \rightarrow \infty$ and so the pion scattering amplitude we obtain is (up to a normalization factor, of course)

$$A(s, t) = \left[\frac{t}{M_C^2}\right]^2 \left[\frac{s}{t+M_C^2}\right]. \tag{3.63}$$

It might be tempting to interpret the first factor as related to the Adler zeroes that should occur at zero four momentum for each pion. However, our analysis has been carried

through with the constraint that $k^2 (= -t) \gg M_C^2$ and so Eq. (3.63) cannot be used at $t=0$. Because of the ϵ tensor that appears in the current coupling, it is the transverse (with respect to the Regge limit) component of each of the p_i that contributes to the factor of t . It is natural, therefore, that if the pions acquire a mass m_π we will have, when all pions are on shell,

$$\left[\frac{t}{M_C^2}\right]^2 \rightarrow \left[O\left(\frac{m_\pi^2}{M_C^2}\right)\right]^2. \tag{3.64}$$

The massive SU(2) singlet gluon Reggeizes in higher orders, with an infrared finite trajectory $\alpha_g(t)$ that satisfies $\alpha_g(M_C^2) = 1$. Also, since we consider the exchange of four transverse momentum gluons, when we add all diagrams only the even signature amplitude will survive. (Indeed, it is argued in [14] that only even signature exchanges can couple via the anomaly.) Therefore, as we add all diagrams and go to higher orders we anticipate that we will have

$$\left[\frac{s}{t+M_C^2}\right] \rightarrow \left[\frac{s^{\alpha_g(t)} + (-s)^{\alpha_g(t)}}{t+M_C^2}\right] \tag{3.65}$$

and so there will be no pole at $t + M_C^2 = 0$. Nevertheless, Reggeized gluon exchange will provide the leading contribution to the Pomeron. It is interesting, of course, that only the quark (or the antiquark) carries the lightlike momentum of the pion that produces the high-energy behavior. This is determined by the generation of the anomaly pole via an internal light-cone momentum, and we comment further on this below.

The factor of

$$\left[\frac{sq^2}{M_C^4} \right] \quad (3.66)$$

is off-shell energy dependence that could be naturally canceled by off-shell propagators. Finally, we note that the factor of

$$\left[\frac{C^2 q^2}{M_C^2} \right]^{14} \quad (3.67)$$

is a wee gluon contribution, with Cq being the boosted longitudinal momentum of wee gluons that in the finite momentum frame have vanishing momentum, orthogonal to the fast quark. In higher orders this contribution will include sums of $|M_N^0|^2$ integrals as factors, where M_N^0 appears in Eq. (3.14) and contains diagrams of the form illustrated in Fig. 7. To say more about this factor it is probably necessary to decouple the mass-shell and Regge limits by performing the full multi-Regge calculation discussed above.

L. The parton amplitude and color confinement

We have emphasized that the exponentiation of infrared divergences already selects color zero transverse momentum states but that this is not confinement because color zero massless multigluon states still contribute at zero Q^2 . However, if the complete set of physical amplitudes is defined via the presence of the overall infrared divergence we have described then there will be both confinement and chiral symmetry breaking. This is because the massless multigluon states will contribute only via the condensate and the initial and final states must be Goldstone bosons for the divergence to be present. Although we have not kept color factors we can make the following comments about how color confinement is realized.

In the original diagrams of the form of Fig. 16(a) the color factors have all of the complexity of the γ -matrix structure illustrated in Figs. 24 and 26. After removal of the color singlet divergent gluons, however, the remaining amplitude necessarily describes SU(2) color zero scattering. In this amplitude, we can interpret the flavor anomaly as unlocking the quark content of a pion via a dynamical fluctuation of the Dirac sea (i.e. the zero momentum chirality transition). This fluctuation produces a “hard” quark carrying all the light-cone momentum together with a wee gluon condensate and an antiquark. The antiquark carries only a soft momentum and is also, essentially, a “wee parton.” It has been produced out of the Dirac sea via a chirality transition that is compen-

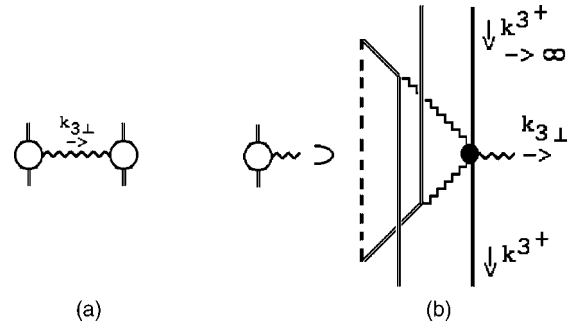


FIG. 27. (a) The parton amplitude; (b) the parton interaction.

sated for by the (effectively classical) background gluon field.

The full amplitude can be represented, as in Fig. 27(a), by simple massive gluon exchange between the fast quarks. This “parton interaction” produces all the transverse momentum that is exchanged. The quark-gluon coupling is not, however, a normal perturbative interaction. Although, as illustrated in Fig. 27(b), it can be computed (“semi”) perturbatively. Accompanying the hard quark interaction, there is a soft interaction in which the slow antiquark, ultimately, is absorbed into the condensate. It is replaced by another antiquark produced out of the condensate. The production and absorption being mediated by a further zero momentum quark chirality transition (shown as the double-dashed line). During the interaction (which we have redrawn compared to earlier figures to make its structure more transparent) color and spin structure, but not momentum, is fed into the fast quark-gluon coupling [the massive gluons can carry SU(2) color]. The spin structure input transforms this coupling from a vector to an axial vector coupling. This being made possible by the chirality transition of the zero momentum quark. The input of color into the fast quark interaction helps convert the odd-signature single gluon exchange to even signature.

An outgoing fast quark carries color, which is neutralized by a (condensate produced) soft antiquark. The Dirac sea completes the confinement by locking the pairs back into a massless Goldstone boson pion via a final zero momentum chirality transition of the soft antiquark that is accompanied by the disappearance of the background “classical gluon field.” Apparently then, in the infinite momentum frame, a physical pion contains a hard elementary quark plus a color compensating “unphysical antiquark” that is described by an antiquark field, but with the Dirac sea shifted. Conversely the quark-antiquark constituents of a pion cannot be liberated without an accompanying gluon field that is responsible for moving the Dirac sea back to its perturbative location. That the dynamical participation of the Dirac sea frees and confines infinite momentum frame quarks (and also modifies interactions) in this manner is natural if in a finite momentum pion the quarks are confined by a nonperturbative adjustment of the Dirac sea, as proposed by Gribov [29]. Since no strong force between quarks is involved, Dokshitzer [30] has called this “soft and gentle confinement.” He has argued for some time that significant experimental evidence for this form of confinement is provided by the momentum proper-

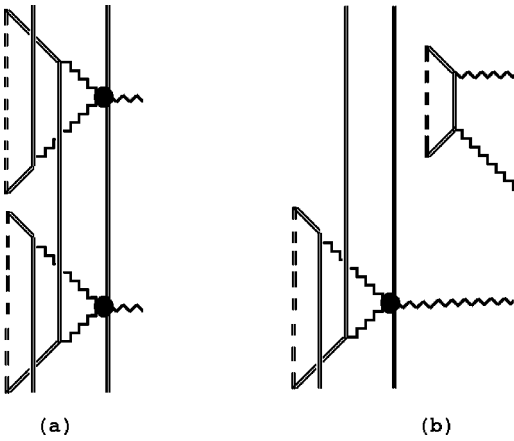


FIG. 28. (a) A two Pomeron vertex; (b) a supercritical vertex?

ties of multihadron production. Since there appears to be very little momentum reordering in the transition from quarks to pions, confinement must take place in a soft and gentle manner. A readjustment of the Dirac sea of the soft quarks-antiquarks that combine with the hard quarks to form hadrons should have just this property.

M. The supercritical Pomeron

In higher orders more massive gluons will be exchanged and more wee quark-antiquark pairs will input additional structure into the interaction. An example of a coupling that will produce two Pomeron exchange is shown in Fig. 28(a). We also expect to find vertices, of the form shown in Fig. 28(b), which include a pair of massive gluons produced by a wee gluon interaction only. To have the axial vector structure for the anomaly, the produced gluon represented by the diagonal element cannot have the polarization to be exchanged in the scattering process. The wee gluon interaction can, however, take place sufficiently far across the rapidity axis that it leads to particle pole interactions within Pomeron vertices, just as is expected in the supercritical Pomeron phase [2]. Since the Pomeron is also exchange degenerate with the Reggeized gluon, all features of supercritical RFT appear to be present.

IV. DISCUSSION

The analysis of this paper demonstrates clearly how (at least the zero momentum part of) the spectral flow of the Dirac sea, which does not enter in standard perturbation theory, enters the (multi-)Regge region interactions that describe the scattering of bound states. The manifestation of this spectral flow is the chirality transition that a zero momentum propagator undergoes in producing the anomaly pole. While we had formulated the basic physics of this phenomenon in our previous papers, we had been unable to find a simple starting point to begin to calculate amplitudes in a sufficiently well-defined way. In the new approach presented in this paper the wee gluon content of Goldstone bosons, produced by the flavor anomaly, provides this starting point. The rotation of the wee gluons during the scattering process introduces, essentially, the triple-Regge kinematics needed

for the U(1) anomaly interactions to appear. As we noted in [14], because of chirality conservation the anomaly interactions cancel, even when the kinematics allow their presence, if the scattering states are elementary quarks or gluons. In contrast, since the initial wee gluon coupling of the pion pole involves a chirality transition, there is no reason for the chirality transitions to cancel in the subsequent scattering.

As has become apparent, our “new approach” is not actually logically separate from the multi-Regge formalism used in our previous papers. Rather it is, essentially, a shortcut that reproduces multi-Regge results without doing the full calculation. The basic idea we have used is that the internal light cone momenta of the flavor anomaly couplings introduce all the large light-cone momenta needed, in addition to the elastic scattering Regge limit, and so this avoids the introduction of complicated multi-Regge limits. This has enabled us to keep the kinematics “relatively” simple. However, we have had to supplement our analysis with additional constraints that appear artificial but really just introduce features that would be provided directly by an underlying multi-Regge limit. The “axial vector currents” to which our Goldstone bosons have coupled are not local currents but rather effective local current components that would be produced by a nonlocal infinite momentum interaction. Such current components appear naturally within a multi-Regge amplitude.

We have described the formation of amplitudes in terms of transverse momentum diagrams that can be thought of, initially, as originating from particular Feynman diagrams. However, many of the integration regions in the Feynman diagrams are cut-off, or even removed altogether. Again multi-Regge theory provides the underlying justification. To have all the necessary anomaly effects present the initial diagrams must be extremely complicated. Remarkably, though, after infrared divergences are extracted and the anomaly contributions isolated, almost all of the complexity disappears and the physical pion scattering amplitude has the very simple structure we have described. Although we have not discussed combining diagrams to obtain explicit color and signature factors it is clear that, in first approximation, the Pomeron is a Regge pole with the same trajectory as a massive, Reggeized, gluon just as we anticipated in our multi-Regge work.

It is amusing (and there may also be deeper implications) that a complete calculation of the multi-Regge S matrix would not be necessary to obtain our results. It would be sufficient to calculate the eight-point amplitude for W^\pm and Z^0 vector mesons in which the scattering of Reggeized pions occurs. The Reggeized pion scattering amplitude could be factorized out and the on-shell amplitude we discuss would be obtained by continuing this amplitude from a spacelike to a lightlike pion mass. In the language of the present paper this implies that the wee gluon structure of a pion is best understood if it is obtained as a wee parton component of an infinite momentum, elementary, vector meson.

We believe that in the multi-Regge framework the existence of a Reggeon condensate in color superconducting QCD would clearly be a derived result. In addition, Reggeized Goldstone bosons would be the only composite

states obtained. The arguments of [15] imply that if the initial Reggeon states are color zero Goldstone bosons the overall logarithmic divergence will produce final states only of this kind. That is, there should be a completeness relation. In this case, the condensate (or rather the infrared divergences and anomalies that produce it) can be said to be responsible for confinement and chiral symmetry breaking. Conversely, the quark content of a pion or nucleon is “liberated” only if it is accompanied by an (effectively classical) gluon background “condensate” that is associated with a shift of the (zero momentum part of) the Dirac sea. The implication being that, at infinite momentum, quarks are locked inside a hadron by a relatively simple spectral flow of the Dirac sea. This form of confinement would have a natural connection with the finite momentum Dirac sea confinement proposed by Gribov [29].

As we have described in more detail in other places [15,9], we expect that SU(3) color is obtained by critical Pomeron behavior [10] that randomizes the SU(2) direction of the condensate within SU(3), while also decoupling the massive Reggeized gluon, as it becomes massless. Thus providing complete SU(3) confinement. The shifting of the Dirac sea that produces confinement then becomes a completely dynamical part of the Pomeron, and hadrons, that has no simple “classical” component. With the better understanding and explicit calculational ability that the results of this paper demonstrate, we should be able to directly identify the higher-order superconducting pion amplitudes with those of supercritical RFT and so establish the connection between the critical Pomeron [10] and QCD. A further implication will be that the physical states of QCD (or rather those that scatter via the physical Pomeron) are either chiral symmetry breaking Goldstone bosons (pions) or contain, as a component, a two quark state that is a Goldstone boson in the color superconducting theory (nucleons). Conversely, the very nature of the Pomeron will be determined by chiral symmetry breaking.

A basic implication of our general program has always been that the Regge limit of QCD, including those properties that are a consequence of confinement and chiral symmetry breaking, would be reachable by essentially perturbative calculations—with the dynamical participation of the Dirac sea being the only extra ingredient. The results of this paper emphasize this implication. According to our results, the only nonperturbative element in color superconducting high-energy amplitudes is the wee-gluon condensate which can be directly understood as a consequence of the all-orders summation of transverse momentum infrared divergences that couple via anomalies (together with the introduction of ultraviolet cutoffs). We should note that the condensate is associated with wee gluon configurations that have the same quantum numbers as the winding number current. Although, as with the currents we use to obtain the flavor anomaly, they are really infinite momentum local current components that result from nonlocal interactions. Nevertheless, there could be a parallel with the Schwinger model where the existence of a condensate can be obtained either by summing diagrams [31] or via nonperturbative topological contributions [32]. However, the topology would have to be in the infinite momentum frame. (Perhaps a winding number for Wilson loop

operators in the transverse plane—this might give a direct analogy with the Schwinger model.)

We have emphasized that, in order to construct high-energy superconducting QCD as we described, it is necessary to introduce cutoffs both in the transverse momenta and in the internal momenta of diagrams that generate anomalies. In effect, these cutoffs regulate the relative infrared-ultraviolet spectral flow of the Dirac sea that is due to the chiral and U(1) anomalies. That all cutoffs can be consistently removed, and the necessary critical behavior retained, is a highly nontrivial requirement which, as we have discussed elsewhere [9,3], is likely to significantly restrict the quark content of QCD. However, it is possible (if not likely) that the very existence of a hadron S matrix within QCD requires that asymptotic freedom, and the consequent perturbation theory, have the maximal applicability. Since parton model cross sections rise asymptotically, this is likely to imply that all physical cross sections must rise asymptotically. The critical Pomeron is well known to be the only description of such cross sections that satisfies all (s - and t -channel) unitarity properties. Consequently, the occurrence of the critical Pomeron in QCD may actually be a necessary requirement for the existence of a hadron S matrix.

The nonperturbative formulation of a gauge theory is generally presumed to be via some form of Euclidean functional integral. In this framework color confinement (as it is usually formulated and studied) is completely disjoint from perturbation theory. In fact, the general expectation is that there will be a “nonperturbative” Pomeron that is crucially dependent on confinement and, as such, is far removed from perturbation theory. However, the Regge region involves a mixture of large light-cone and small transverse momenta and so appears only in Minkowski space. As a consequence, if the Euclidean path integral is the starting point, detailed properties of the Pomeron can only be determined by a complete nonperturbative solution of the theory from which Minkowski space hadron scattering amplitudes can be extracted and the Regge limit taken. Something that seems unlikely to be possible for a very long time to come. Indeed, given that a complete nonperturbative solution of QCD has been found, the Pomeron would probably be one of the last things to be studied. Note that, since light-cone momentum regions become all important as the continuation to Minkowski space is made, the very existence of this continuation is likely to be contingent on the existence of (unitarity?) boundedness properties in the Regge region.

We would like to emphasize that there is no guarantee that a Minkowski region unitary S matrix can be derived from a nonperturbative Euclidean path integral—particularly given the complexity [23] of the, large field, unphysical degrees of freedom that are present. (Indeed a commonly agreed procedure to definitively eliminate these degrees of freedom has not yet been found.) The demonstrated perturbative unitarity [24] is only a formal property since infrared divergences prevent the existence of a finite S matrix. There is certainly no understanding of how the unitarity properties of the perturbative theory might translate into unitarity with respect to a nonperturbative physical spectrum that manifests confinement and chiral symmetry breaking. Indeed it is our strong

belief that the Regge region must play a special role in unraveling this relationship within QCD. Since small transverse momenta are involved, the physical properties of confinement and chiral symmetry breaking must be evident in the t -channel unitarity condition. Conversely, if asymptotic freedom has maximal applicability, the involvement of large momenta should imply that the Pomeron is not too far from perturbation theory. Therefore, the (multi-) Regge region should provide a unique possibility to understand the relationship between perturbation theory and the physical states appearing in the unitarity condition.

If the Regge limit of QCD can be constructed by the essentially perturbative methods we describe then the unitarity properties of massive quark and gluon Reggeon diagrams

translates into similar properties for the Pomeron and hadron Reggeon diagrams. The unitarity of the critical Pomeron will be clearly related to the original perturbative unitarity of quarks and gluons. Indeed it could also be that, since the construction stays so close to perturbation theory, the problem of eliminating large field unphysical degrees of freedom will have been avoided.

ACKNOWLEDGMENTS

This work was supported by the U.S. Department of Energy, Division of High Energy Physics, Contracts W-31-109-ENG-38 and DEFG05-86-ER-40272.

-
- [1] V.N. Gribov, I.Ya. Pomeranchuk, and K.A. Ter-Martirosyan, *Phys. Rev.* **139**, B184 (1965).
- [2] A.R. White, *Int. J. Mod. Phys. A* **6**, 1859 (1991).
- [3] A.R. White, in *Scattering*, edited by E.R. Pike and P. Sabatier (Academic, New York, 2002), hep-ph/0002303.
- [4] V.S. Fadin, E.A. Kuraev, and L.N. Lipatov, *Sov. Phys. JETP* **45**, 199 (1977).
- [5] J.B. Bronzan and R.L. Sugar, *Phys. Rev. D* **17**, 585 (1978); this paper organizes into Reggeon diagrams the results from H. Cheng and C.Y. Lo, *ibid.* **13**, 1131 (1976); **15**, 2959 (1977).
- [6] V.S. Fadin and V.E. Sherman, *Sov. Phys. JETP* **45**, 861 (1978).
- [7] V.S. Fadin and L.N. Lipatov, *Nucl. Phys.* **B477**, 767 (1996) and further references therein.
- [8] J. Bartels, *Z. Phys. C* **60**, 471 (1993) and further references therein.
- [9] A.R. White, *Int. J. Mod. Phys. A* **8**, 4755 (1993).
- [10] A.A. Migdal, A.M. Polyakov, and K.A. Ter-Martirosyan, *Zh. Eksp. Teor. Fiz.* **67**, 84 (1974); H.D.I. Abarbanel and J.B. Bronzan, *Phys. Rev. D* **9**, 2397 (1974).
- [11] A.R. White, *Phys. Rev. D* **29**, 1435 (1984).
- [12] A. R. White, CERN Report No. TH.2976 (1980). A summary of this paper is presented in the Proceedings of the XVIth Rencontre de Moriond, Vol. 2 (1981).
- [13] A.R. White, *Phys. Rev. D* **66**, 045009 (2002).
- [14] A.R. White, *Phys. Rev. D* **63**, 016007 (2001).
- [15] A.R. White, *Phys. Rev. D* **58**, 074008 (1998); *Nucl. Phys. B (Proc. Suppl.)* **96**, 277 (2001); see also Lectures in the Proceedings of the Theory Institute on Deep-Inelastic Diffraction, Argonne National Laboratory (1998).
- [16] P. Goddard and A.R. White, *Nucl. Phys.* **B17**, 1 (1970); **B17**, 45 (1970).
- [17] G. 't Hooft, in *Recent Developments in Gauge Theories*, edited by G. 't Hooft *et al.* (Plenum, New York, 1980).
- [18] S. Coleman and B. Grossman, *Nucl. Phys.* **B203**, 205 (1982).
- [19] T. Banks, Y. Frishman, A. Schwimmer, and S. Yankielowicz, *Nucl. Phys.* **B177**, 157 (1981).
- [20] J. Horejsi, *Czech. J. Phys., Sect. B* **35**, 820 (1984).
- [21] N.N. Achasov, *Phys. Lett. B* **287**, 213 (1992).
- [22] J.B. Kogut, M.A. Stephanov, D. Toublan, J.J.M. Verbaarschot, and A. Zhitnitsky, *Nucl. Phys.* **B582**, 477 (2000).
- [23] V.N. Gribov, *Nucl. Phys.* **B139**, 1 (1978); G. 't Hooft, *Nucl. Phys. B (Proc. Suppl.)* **74**, 413 (1999).
- [24] G. 't Hooft, *Nucl. Phys.* **B33**, 173 (1971).
- [25] S.I. Adler and W.B. Bardeen, *Phys. Rev.* **182**, 1517 (1969).
- [26] V.S. Fadin and L.N. Lipatov, *Nucl. Phys.* **B406**, 259 (1993).
- [27] A. Sen, *Phys. Rev. D* **27**, 2997 (1983) and unpublished work on non-Abelian gauge theories.
- [28] R. Kirschner, L. Mankiewicz, A. Schafer, and L. Szymanowski, *Z. Phys. C* **74**, 501 (1997); a more general reference for light-cone γ -matrix and coordinate manipulations is S.J. Brodsky and G.P. Lepage, *Phys. Rev. D* **22**, 2157 (1980).
- [29] V.N. Gribov, *Eur. Phys. J. C* **10**, 71,91 (1999).
- [30] Yu.L. Dokshitzer, *Philos. Trans. R. Soc. London* **A359**, 309 (2001).
- [31] Y. Frishman, *Lecture Notes in Physics* Vol. 32 (Springer-Verlag, New York, 1975); G.T. Bodwin and E. Kovacs, *Phys. Rev. D* **35**, 3198 (1987).
- [32] N.S. Manton, *Ann. Phys. (N.Y.)* **159**, 220 (1985); see also G.S. Danilov, I.T. Dyatlov, and V.Yu. Petrov, hep-th/9512049 and references therein.